Heat and freshwater changes in the Indian Ocean region

Caroline C. Ummenhofer[1,2]✉, *Sujata A. Murty*[1,3], *Janet Sprintall*[4], *Tong Lee*[5] *and Nerilie J. Abram*[6,7]

Abstract | Across the Indo-Pacific region, rapid increases in surface temperatures, ocean heat content and concomitant hydrological changes have implications for sea level rise, ocean circulation and regional freshwater availability. In this Review, we synthesize evidence from multiple data sources to elucidate whether the observed heat and freshwater changes in the Indian Ocean represent an intensification of the hydrological cycle, as expected in a warming world. At the basin scale, twentieth century warming trends can be unequivocally attributed to human-induced climate change. Changes since 1980, however, appear dominated by multi-decadal variability associated with the Interdecadal Pacific oscillation, manifested as shifts in the Walker circulation and a corresponding reorganization of the Indo-Pacific heat and freshwater balance. Such variability, coupled with regional-scale trends, a short observational record and climate model uncertainties, makes it difficult to assess whether contemporary changes represent an anthropogenically forced transformation of the hydrological cycle. Future work must, therefore, focus on maintaining and expanding observing systems of remotely sensed and in situ observations, as well as extending and integrating coral proxy networks. Improved climate model simulations of the Maritime Continent region and its intricate exchange between the Pacific and Indian oceans are further necessary to quantify and attribute Indo-Pacific hydrological changes.

Indo-Pacific warm pool (IPWP). Region at the intersection of the Indian and Pacific oceans, defined as the area with annual sea surface temperature above 28 °C (FIG. 1b), coinciding with the rising branch of the Walker circulation.

Ocean heat content (OHC). The quantity of heat stored in the ocean, proportional to temperature integrated vertically over a prescribed depth range.

Internal variability Climate variability that arises due to natural processes or interactions between various components of the climate system, as opposed to anthropogenic or external forcing.

✉e-mail: cummenhofer@whoi.edu

https://doi.org/10.1038/s43017-021-00192-6

The oceans form an integral part of the global hydrological cycle[1,2], with the oceanic, atmospheric and terrestrial components linked through atmospheric moisture transport and continental runoff[3]. Ocean salinity is a key metric in this exchange, tracking and temporally integrating characteristics of the hydrological cycle, elevating small trends in atmospheric forcing to a detectable level. Indeed, global patterns of sea surface salinity (SSS) trends since the 1950s[4–6] provide evidence for an intensification of the hydrological cycle — that is, a freshening of rainfall-dominated tropical atmospheric convergence regions, such as the warm and fresh Indo-Pacific warm pool (IPWP) and a salinification of evaporation-dominated subtropical regions[6] — as expected in a warming climate[7].

The Indian Ocean stands out as a region that has experienced pronounced warming[8], which raises the question whether a concomitant intensification of the hydrological cycle has already commenced. For example, superimposed against a background of sustained twentieth century surface warming — which exceeds that of other tropical ocean basins[9] — a rapid rise in the ocean heat content (OHC) of the Indian Ocean has been observed since the 2000s[10,11]. At the same time, pronounced changes in the freshwater balance have been apparent, including strong freshening trends over the Maritime Continent (MC) and eastern Indian Ocean.

However, distinguishing anthropogenically forced signals of hydrological intensification can be difficult, owing to many confounding factors. For instance, internal variability, particularly that associated with modes of variability such as the Indian Ocean Dipole (IOD) and remote influences of the El Niño–Southern Oscillation (ENSO) also influence the Indo-Pacific hydroclimate. These modes are not stationary[12–15] and, instead, vary on multi-decadal timescales and beyond[15–20]. Constraining Pacific multi-decadal variability such as associated with the Interdecadal Pacific oscillation (IPO) is, thus, critical for predicting future changes in Indo-Pacific hydroclimate. Moreover, limitations of the observational record in space and time (BOX 1), and shortfalls in coupled climate models regarding their resolution and representation of key processes (BOX 2), add to the challenge to quantify and attribute heat and freshwater changes in the Indian Ocean.

Yet, determining whether contemporary trends represent a manifestation of multi-decadal variability or an anthropogenic intensification of the hydrological cycle has important implications for climate predictions and risk planning across the region. Heat and freshwater

Key points

- At the basin scale, the Indian Ocean sustained robust twentieth century surface warming exceeding that of other tropical ocean basins. Yet, substantial variability exists regarding the magnitude and confidence in trends at regional scales, especially in the subsurface, due to the sparse observational network.
- Indian Ocean heat content has risen rapidly since the 2000s and concomitant freshening occurred over the eastern Indian Ocean and Maritime Continent (MC).
- Broad-scale warming and MC freshening trends are consistent with expected changes of an intensifying hydrological cycle in a warming world; however, the rate of observed change since the 1980s likely results from natural multi-decadal variability associated with the Interdecadal Pacific oscillation.
- Disentangling the effects of multi-decadal natural variability and anthropogenic change on heat and freshwater changes in the Indian Ocean and MC region — of importance for climate risk assessments for vulnerable societies in Indian Ocean rim countries — require sustained and enhanced observations.
- Centennial trends based on coral proxies indicate robust warming and freshening since the 1850s over the Indian Ocean and broader MC region. However, the reconstructed century-scale trend magnitude is much lower than the rapid trends observed since 1980, which were most likely exacerbated by recent acceleration of anthropogenic climate warming and natural multi-decadal variability associated with Interdecadal Pacific oscillation phase shifts.
- Quantifying change in the Indian Ocean heat and freshwater balance warrants a multi-pronged approach that capitalizes on a systematic integration of in situ observations, remote sensing, numerical modelling efforts and palaeo proxy networks across temporal and spatial scales.

changes affect patterns of regional sea level rise and Indo-Pacific ocean circulation[21–23]. Warming ocean temperatures further enhance hydrological variability[7,24], contributing to rainfall extremes[25–31]. Any changes in oceanic evaporation could also increase its contribution to terrestrial precipitation[32,33], with implications for societally relevant water resources across Indian Ocean rim countries, whose mainly agrarian societies rely on sufficient rainfall and are vulnerable to drought and floods.

In this Review, we synthesize current understanding of Indian Ocean heat and freshwater changes at decadal to multi-decadal timescales to ascertain whether a hydrological intensification has occurred. We highlight the distinct characteristics of the Indian Ocean's heat and freshwater balance, as well as how they are modulated by local and remote drivers on interannual to multi-decadal and centennial timescales. The observed changes since the 1980s in heat and freshwater over the broader Indian Ocean region are evaluated using different data sources, with a specific focus on the MC region and on whether changes appear dominated by natural variability and/or are consistent with expected changes from an anthropogenically forced signal. Finally, we use coral proxies to provide a long-term context and an opportunity to elucidate how contemporary observed changes fit with hydroclimatic trends recorded throughout the nineteenth and twentieth centuries. We finish by highlighting outstanding challenges and future research priorities.

Modes of variability
Natural, recurrent climate phenomena with an underlying space-time structure that displays a preferred spatial pattern and temporal variation in components of the climate system (e.g. ocean, atmosphere and cryosphere).

Indian Ocean Dipole
(IOD). Coupled ocean–atmosphere phenomenon in the tropical Indian Ocean peaking in boreal fall, with its positive phase characterized by anomalous cooling (warming) in the tropical south-east (western) Indian Ocean.

Author addresses

[1]Department of Physical Oceanography, Woods Hole Oceanographic Institution, Woods Hole, MA, USA.
[2]ARC Centre of Excellence for Climate Extremes, University of New South Wales, Sydney, NSW, Australia.
[3]Department of Atmospheric and Environmental Sciences, University at Albany, State University of New York, Albany, NY, USA.
[4]Scripps Institution of Oceanography, University of California San Diego, La Jolla, CA, USA.
[5]Jet Propulsion, Laboratory, California Institute of Technology, Pasadena, CA, USA.
[6]Research School of Earth Sciences, The Australian National University, Canberra, ACT, Australia.
[7]ARC Centre of Excellence for Climate Extremes, The Australian National University, Canberra, ACT, Australia.

Indian Ocean climatological conditions

Several unique characteristics distinguish the climatological structure of the Indian Ocean from other tropical ocean basins, influencing its behaviour on seasonal to multi-decadal timescales and beyond[34]: a seasonal reversal of monsoon winds that drive corresponding reversals in the ocean circulation and, thereby, substantial short-term variability; the absence of steady equatorial easterlies that lead to a comparatively deep thermocline in the eastern Indian Ocean; and a low-latitude connection to the Pacific that facilitates substantial heat and freshwater input, paired with an absence of northward heat export, owing to the presence of the Asian continent, which make the Indian Ocean particularly vulnerable to anthropogenic climate change[8], as pathways for heat export from the Indian Ocean are limited.

The low latitude connection is via the Indonesian throughflow (ITF). The ITF connects the western Pacific to the eastern Indian Ocean, with a total average transport of ~15 Sv (1 Sv = 10^6 m^3 s^{-1}; REF.[35]), split across multiple passages and extending throughout the upper 800–1,200 m (REF.[36]). On annual and longer timescales, the ITF is influenced by the Indo-Pacific pressure gradient, itself linked to the large-scale Indo-Pacific wind field[37] and freshwater fluxes that result in buoyancy changes[21–23,38–40]. The ITF accounts for substantial heat and freshwater input to the Indian Ocean, but is not well constrained by direct observations from within the Indonesian seas[41].

The IPWP (FIG. 1) represents another key feature in the region. The IPWP is defined by the 28 °C isotherm and is associated with the ascending branch of the Walker circulation. Accordingly, it is characterized by high climatological mean evaporation and rainfall rates, with the precipitation maximum tapering off towards the western part of the basin (FIG. 1a). Lower precipitation is found in the subtropics, with minimum values evident at ~20–30°S off the coast of Western Australia and in the north-west Arabian Sea[42]. Strong precipitation variations are observed near orographic features (FIG. 1a), as well as in association with monsoon systems, and ENSO and IOD variability[43].

To first order, the observed SSS (FIG. 1b) might be expected to reflect the pattern of evaporation-minus-precipitation, with mismatches suggesting regions where effects from river discharge and ocean dynamics are important. The MC, for example, is relatively fresh, owing to both direct precipitation input from the Walker circulation and Southeast Asian riverine input, for example, from the Mekong River system entering the South China Sea (FIG. 1b). River runoff from the Ganges, Brahmaputra and Irrawaddy river systems — which accounts for 60% of total riverine input north of 30°S (REF.[44]) — further produces the freshest

Box 1 | **Heat and freshwater signals from observations and corals**

Different data sources can provide complementary information about heat and freshwater changes. Direct comparison of linear trends or temporal variability in heat and freshwater metrics arising from different data sources warrants understanding the limitations inherent in the measurement method or its spatiotemporal characteristics.

In situ ocean observations

Historically, the Indian Ocean is the least observed among the major ocean basins[8]. Most temperature measurements in the historical record stem from expendable bathythermographs. Frequently repeated expendable bathythermograph transects resolve the sectional geostrophic velocity and transport, such as the IX1 transect, which measures the Indonesian throughflow as it exits into the Indian Ocean (FIG. 1).

Salinity profiles are particularly sparse, with most historical measurements obtained from conductivity–temperature–depth sensors. The advent of the Argo programme in 2003, however, enabled widespread salinity profiles to be measured; free-drifting profilers with in-built conductivity–temperature–depth sensors profile from 2,000 m depth to the surface every 10 days over a lifespan of 4–5 years.

Mooring deployments permit understanding of oceanic variability on shorter timescales. For example, fixed-site moorings provide a platform to obtain high-resolution property time series, including velocity measurements. In the narrow passages of the Indonesian seas, moored arrays of instruments as part of the 2003–2006 INSTANT and 2006–2019 MITF projects have effectively returned volume and property Indonesian throughflow transport time series[41].

Remote sensing

Since 2010, three passive microwave satellite missions provided synoptic sea surface salinity measurements[186]: Soil Moisture and Ocean Salinity (2010–present), Aquarius (September 2011 to May 2015) and Soil Moisture Active Passive (2015–present). Multiple satellite-derived precipitation estimates are incorporated into the Climate Prediction Center Merged Analysis of Precipitation and Global Precipitation Climatology Project, as well as rain gauges on land[178,187]. The Tropical Rainfall Measuring Mission Multi-satellite Precipitation Analysis[188] combines the Tropical Rainfall Measuring Mission with precipitation measurements from the Global Precipitation Measurement mission core satellite. Precipitation-measuring satellites best detect stronger and more persistent rain[188]. The AVISO sea surface height[171] product merges measurements from 12 satellite altimeter missions since 1992. Sea surface height in coastal areas, especially where strong tides occur, such as in the Maritime Continent, have lower quality compared with that in the open ocean.

Challenges for comparing satellite-derived salinity measurements with in situ observations include differences in sampling scales (40–150-km footprints versus pointwise measurements); differences in measurement depths between satellite-derived fields (for the upper centimetre) and in situ (at ≥5 m); and sparse in situ measurements in coastal regions, where satellite fields are subject to contaminations by man-made radio signals and land signal leakage[189]. The NOAA Optimally Interpolated sea surface temperature (SST) analysis[190] combines measurements from infrared and passive microwave radiometers, blended with in situ SST to help adjust the relative biases.

Observational-based products

Global SST analysis products, such as the NOAA Extended Reconstructed Sea Surface Temperature[177] and Hadley Centre Sea Ice and Sea Surface Temperature[176], combine available SST observations with missing data infilled using statistical methods.

Corals

Corals are important environmental archives of tropical ocean conditions over monthly to centennial timescales[191]. Long-lived massive colonies can yield cores extending back over 400 years and fossil coral specimens allow for reconstructions further back in time. During calcification, minor elements and isotopes are incorporated into the coral skeleton that reflect surrounding seawater composition and environmental conditions. The ratio of stable oxygen isotopes ($^{18}O/^{16}O$ or $\delta^{18}O$) in corals reflects both SST and the $\delta^{18}O$ composition of the surrounding seawater ($\delta^{18}O_{sw}$), which generally has a linear relationship with sea surface salinity[192,193]. Annual density banding patterns distinguishable in X-rays[194] and precise geochemical chronologies further allow records to be compared across large distances[121].

El Niño–Southern Oscillation
(ENSO). Strong year-to-year climate variability originating in the equatorial Pacific Ocean through coupled ocean–atmosphere interactions. El Niño–Southern Oscillation manifests itself in anomalous surface warming (El Niño) or cooling (La Niña) that typically peaks in boreal winter.

Interdecadal Pacific oscillation
(IPO). Decadal mode of Pacific variability (similar to Pacific decadal oscillation) but with a meridionally broader tropical El Niño-like warm temperature anomaly pattern and cool extratropical Pacific during its positive phase.

Thermocline
Zone of maximum vertical temperature gradient, separating warm and cold layers of water. The 20 °C isotherm is often used as an indicator of thermocline depth in the equatorial Indo-Pacific.

surface waters of all the global tropical oceans in the Bay of Bengal (FIG. 1b), resulting in strong salinity stratification in the upper 50–80 m of the region[45,46]. Subsurface salinity patterns in the upper 200 m within the Indian Ocean basin primarily reflect the SSS patterns[47].

Ocean dynamics are important for redistributing the low-salinity waters exiting the Indonesian seas and freshwater owing to local rainfall in the South Indian Ocean. For instance, freshwater advected from the Indonesian seas lowers the salinity from where it enters the south-east Indian Ocean at ~10–15°S from the surface to ~600 m depth all the way across the Indian Ocean to the coast of Madagascar[47–49]. Furthermore, the low surface salinity along 15°S located about 6–8° south of the rainfall maximum is likely contributed through southward Ekman transport in response to the dominant easterly winds found south of 10°S in the Indian Ocean[44]. In addition, the part of the fresh ITF[21] that enters the poleward flowing Leeuwin Current acts to erode the effect of the local evaporation–precipitation maximum, such that relatively low SSS is found against the coast of Western Australia (FIG. 1b). In contrast, the saltiest waters of the Indian Ocean basin are found in the northern Arabian Sea, influenced by the high-salinity inflow from the evaporatively driven marginal Red and Persian seas[50].

Drivers of multi-decadal change

Global mean surface temperatures have steadily risen in response to anthropogenic greenhouse gas emissions[51]. Warming temperatures are expected to result in a combination of local-scale or regional-scale dynamic (driven by atmospheric or oceanic circulation changes) and global-scale thermodynamic (driven by temperature-related changes, including moisture content) responses that affect the hydrological cycle; at times, these act in concert, and, at other times, in opposition. Assessing such theoretical considerations allows observed changes in the heat and freshwater balance to be evaluated against those expected in a warming climate.

Thermodynamic considerations. Thermodynamic responses arise from changes in specific humidity, in particular, a 7% increase in moisture holding capacity per degree of temperature change, as outlined by the Clausius–Clapeyron relation. Thus, even when holding the circulation (or dynamics) constant, wet areas can be expected to get wetter and dry areas drier[7,52,53]. To first order, higher sea surface temperature (SST) might be expected to lead to higher oceanic evaporation, and, by inference, higher precipitation[7,24]. While satellite-derived estimates indicate a 10% increase in global oceanic evaporation over 1978–2005 (REF.[24]),

Box 2 | **Heat and freshwater signals from reanalyses and climate models**

Both reanalysis products and climate model simulations provide gridded, multi-dimensional data of physical and chemical properties of the climate system that can be used to assess heat and freshwater changes across a range of timescales.

Reanalysis products

Reanalyses use data assimilation to combine observations with dynamics represented by numerical models of the ocean or atmosphere to infill gaps or missing variables and produce gridded state estimates[195–197]. Reanalyses face several challenges, including inadequacy of observational constraints related to data coverage, sampling and uncertainty, as well as changes of observing systems; deficiencies in models, including resolution, parameterizations, numerical implementation and missing physics, some of which cause model biases and drift; uncertainties in model forcings; and limitations in data assimilation methods. Data-sparse ocean regions, such as the Indian Ocean, or regions with complex topography as in the Maritime Continent (MC), are areas where high-quality ocean reanalyses are particularly desirable, but are also least constrained by observations. Sparsity of observations is considered the key limitation in furthering observed understanding of the physical world and for validating and improving its representation in models; especially regional seas, continental shelves and near-coastal land–sea interactions lack observations for quantifying budgets for heat and freshwater[148].

Climate models

A numerical representation of the climate system that is based on physical, chemical and biological properties of its components, their interactions and feedback[198]. The climate system can be represented by models of varying complexity; that is, for any one or multiple component(s), a hierarchy of models can be identified, differing in the extent to which processes are explicitly represented, the number of spatial dimensions and resolutions, or the level at which empirical parameterizations are involved. Climate models are used for studying and simulating the climate and for operational purposes, including seasonal, interannual and decadal climate predictions. State-of-the-art climate model simulations are conducted and coordinated through the Coupled Model Intercomparison Project, an international effort of modelling centres that follow common protocols defined to address questions on climate variability and change under the umbrella of the Intergovernmental Panel on Climate Change.

The MC region represents considerable challenges for numerical simulations: complex topography, both regarding its bathymetry with shallow passages and narrow straits within the ocean, as well as strong land–sea thermal gradients between the ocean and numerous islands with steep elevation across the Indonesian archipelago[199]. These compounding factors have implications for oceanic transport and Indo-Pacific heat and freshwater exchange, as well as for complex air–sea interactions that influence the diurnal cycle of convective activity over the islands, with implications for runoff and salinity distribution.

A further challenge is large tidal mixing in the MC region[41], which most models would need to include via a tidal mixing parameterization that is missing in many current-generation ocean reanalyses and climate models, yet, is critical for a realistic representation of the Indonesian throughflow heat and salt flux from the Pacific Ocean to the Indian Ocean.

only small trends in precipitation have been observed over the global oceans[42,54]; these evaporative changes also include the response from enhanced wind speed, rather than only SST, complicating the interpretation. Hence, in observations, internal variability aliases the quantification of such thermodynamic hydrological changes, and, in models, uncertainties in atmosphere–radiation interaction[55] result in weakened Clausius–Clapeyron scaling, typically ~1–3% K^{-1}. Moreover, the 'warmer get wetter' pattern dominates over 'wet gets wetter' in many model simulations (likely as a result of surface warming destabilizing the atmosphere and inducing more upward motion, and, thus, more moisture convergence and rain[56]), leading to spurious rainfall projections[57].These discrepancies between theoretical, observed and modelled hydrological changes suggest that dynamical changes in atmospheric circulation might be important.

Dynamical considerations. The expected dynamical changes to the tropical hydroclimate in a warming world relate to the behaviour of the zonal Walker circulation and its interaction with the upper ocean across the Indo-Pacific. While focus has often been on the Pacific limb of the Walker circulation, the intricate nature of the tropical circulation spanning the Indo-Pacific[58] suggests that any changes would also be transmitted to and affect the Indian Ocean sector. For example, changes in the Pacific Walker circulation can induce an oceanic response that results in planetary waves and thermocline displacements that are transmitted via the Indonesian seas and the ITF[34]. The atmospheric bridge can also mediate shifts of the Indian Ocean component of the tropical Walker circulation[58]. The strengths of these relationships are likely not stationary over time[59]. As the Walker circulation's ascending branch is located over the IPWP and one of its downward branches over the western Indian Ocean, any shifts in the position or strength of either branch translates to substantial modifications of the Indian Ocean freshwater balance.

Based on theoretical considerations, coupled climate models and observational evidence, the Walker circulation is expected to weaken in a warming world, owing to differential rates of precipitation and water vapour change in response to surface warming[60,61]. That is, as the tropical oceans warm, rainfall increases over the wet IPWP, but less rapidly than atmospheric water vapour. Through continuity, the inflow of atmospheric moisture, therefore, slows[62]. This secular slowdown in the zonal Walker circulation and related zonal pressure gradient, in turn, weakens the strength of the equatorial easterly trade winds across the Pacific, resulting in a weakening of the equatorial SST and thermocline gradient in the Pacific[60,63,64]. Over the Indian Ocean sector, enhanced surface warming in the west compared with the east[65], along with a progressive shoaling of the eastern Indian Ocean thermocline for the second half of the twentieth century, were seen as consistent with a slowdown of the Walker circulation[12,13,66].

However, subsequent observational evidence has not supported the expected weakening of the Walker circulation or corresponding signatures in tropical Pacific winds[67,68], Indo-Pacific sea surface height (SSH) patterns[69] or the equatorial Pacific thermocline gradient[70]. Instead, such metrics have shown the opposite effect, that is, a strengthening of the Walker circulation, contradicting expected secular changes based on climate models. Debate persists regarding the cause of this discrepancy, but data-set dependencies[63,64,71] and artefacts of residual trends from ENSO variability[65,72] have been given as possible causes. Yet, it has now been suggested that the observed strengthening of the equatorial thermocline gradient in the Pacific is consistent with climate models when accounting and correcting for persistent spurious cold tongue biases that are common in Coupled Model Intercomparison Project (CMIP)-class climate models[73]. Furthermore, the strong surface warming observed over the Indian Ocean has been proposed to have contributed to the Walker circulation's strengthening over the Pacific sector[59] through a remote thermostat mechanism[74]. The tug of war between ocean

Indonesian throughflow
(ITF). Ocean currents from the Pacific Ocean to the Indian Ocean through the passages of the Indonesian archipelago.

Walker circulation
Thermally driven tropical zonal overturning atmospheric circulation associated with rising (sinking) air over the Indo-Pacific warm pool (eastern Pacific), undergoing substantial longitudinal shifts in location in response to the El Niño–Southern Oscillation, Indian Ocean Dipole, and Interdecadal Pacific Oscillation.

Ekman transport
Lateral movement of water in the frictional boundary layer of a fluid, directed to the right or left of the wind in the Northern or Southern Hemisphere, respectively, because of the Coriolis force.

Leeuwin Current
Poleward-flowing eastern boundary current off the west coast of Western Australia that transports relatively warm and fresh waters southward.

Teleconnections
Changes in atmospheric or oceanic circulation over widely separated, geographically fixed spatial locations; often a consequence of large-scale wave motions, whereby energy is transferred from source regions along preferred atmospheric/oceanic paths.

La Niña
The cold phase of the El Niño–Southern Oscillation, characterized by anomalous surface cooling and stronger trade winds in the equatorial Pacific Ocean.

thermostat and atmospheric dynamic responses — leading to an accelerated or weakened Walker circulation, respectively — might be timescale-dependent, the former arising from a strengthened zonal SST gradient representing a fast response to anthropogenic greenhouse gases and the latter representing a slower response involving extratropical oceanic teleconnections[75].

Multi-decadal variability associated with the IPO. At a global or basin scale, superimposed on the secular warming trend is considerable multi-decadal variability. This variability includes periods of relatively low or near-zero warming — so-called global warming hiatus periods — as occurred from the late 1990s to about 2012 (REFS[76,77]). During the hiatus, surface temperatures increased more slowly, while surplus heating continued to warm the subsurface ocean, as evident from robust OHC increases[77].

The hiatus coincided with a negative phase of the IPO in the Pacific, and it is believed that the IPO-related reorganization of the Indo-Pacific climate system had a substantial role in changing the regional heat and freshwater balance[10,11,78–80]. Much like La Niña, negative phases of the IPO are characterized by enhanced equatorial trade winds and cooler SST in the eastern Pacific and warmer SST in the IPWP[68]. Changes in the horizontal SST gradient subsequently strengthen and shift the Walker circulation further westward from its climatological position[81]. These Indo-Pacific circulation changes enhance the redistribution of heat from the

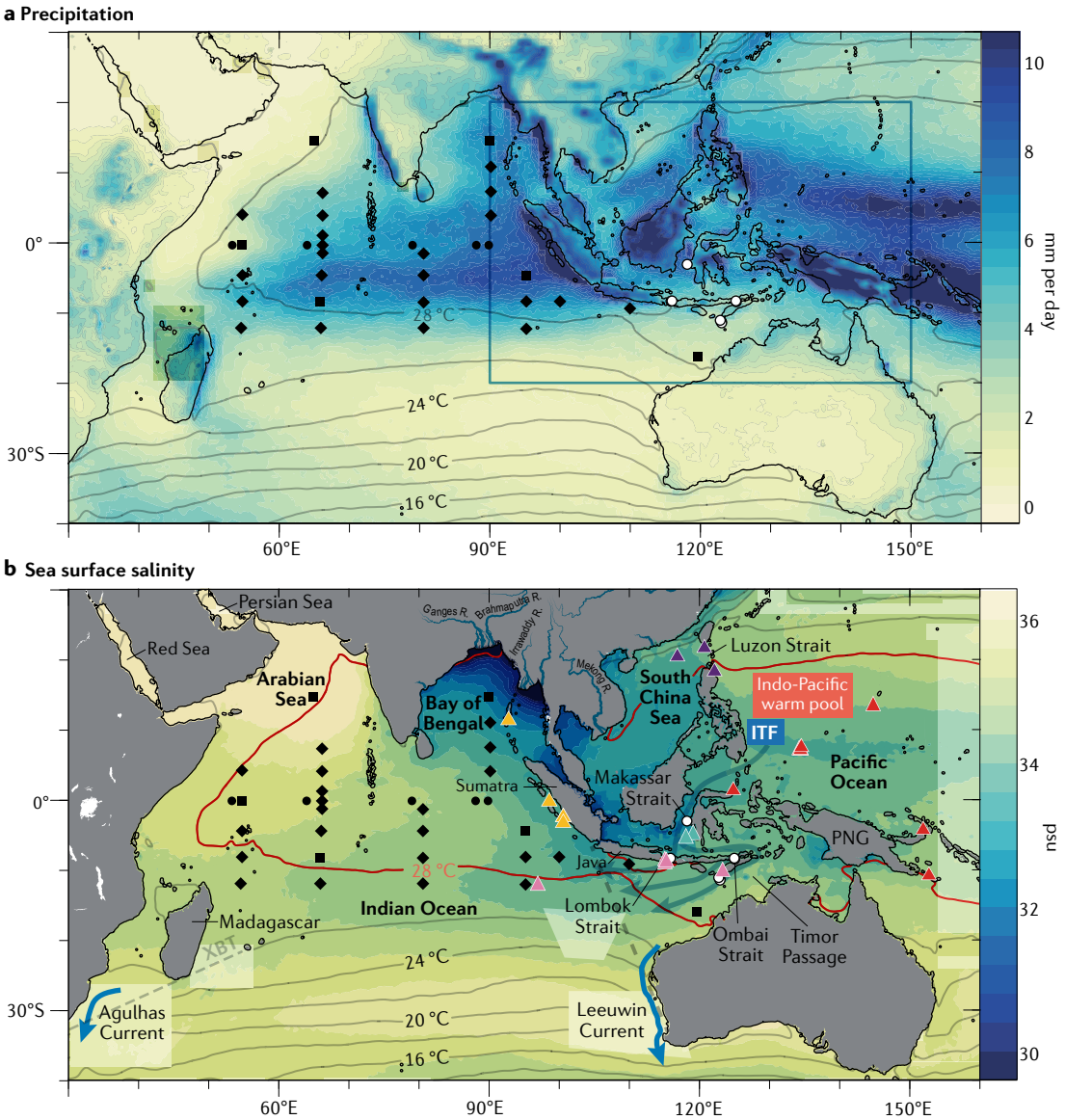

Fig. 1 | **Mean precipitation and surface ocean temperature and salinity conditions.** Annual mean precipitation[168] (panel **a**), sea surface salinity[169] (panel **b**) and sea surface temperature[170] (contours, both panels) calculated over 2010–2019. The blue box in panel **a** indicates the region used for spatial averaging in FIGS 3,5. Black symbols indicate locations of the RAMA array[8]. White circles indicate locations of the INSTANT array[35]. In panel **b**, grey lines and coloured symbols indicate key expendable bathythermograph (XBT) lines and sites of coral proxy records, respectively. ITF, Indonesian throughflow; PNG, Papua New Guinea; R., river.

El Niño
The warm phase of the El Niño–Southern Oscillation, characterized by anomalous surface warming and weaker trade winds in the equatorial Pacific Ocean.

Argo
International programme that collects subsurface ocean property measurements using a fleet of robotic instruments that profile between the surface and a mid-depth level (1,000–2,000 m) and then drift with the ocean currents.

neighbouring Pacific through the Indonesian archipelago via the ITF[10,11,79,82–84] and into the Indian Ocean. Positive IPO phases, much like El Niño, have the converse conditions and effects.

Opposing phases of the IPO can also modulate heat transport and influence the background state of the eastern Indian Ocean thermocline. The latter has important implications for the frequency of IOD events: during positive IPO phases, the eastern Indian Ocean thermocline is relatively shallow, resulting in more positive and fewer negative IOD events per decade, while the opposite occurs during negative IPO phases favouring a deeper thermocline[15,19,20]. As such, multi-decadal variability associated with the IPO can interact and modulate the frequency of interannual variability associated with the IOD. Yet, how Pacific surface forcing and interbasin exchanges with the Indian Ocean are apportioned through different pathways is less clear, whether via the ocean, the atmosphere or a combination of the two[85].

At the broad scale, there is general agreement on patterns of hydroclimatic change arising from these dynamic and thermodynamic changes[4,6,7,52], albeit with low confidence[53]. For example, these changes include enhanced precipitation and freshening in monsoon-dominated regions in the northern Indian Ocean and tropical atmospheric convergence zones, such as over the MC region. The changes likely arise from a combination of thermodynamic (atmospheric-moisture-related) and dynamic (circulation-driven changes as associated with the Walker circulation) processes, compounded by an IPO phase shift from positive (~1978–1998) to negative (~1999–2015) that similarly manifests as shifts in the Indo-Pacific Walker circulation and the resultant footprint in the heat and freshwater balance over the eastern Indian Ocean and MC region.

Contemporary heat and freshwater trends

Given the robust twentieth century surface warming in the Indian Ocean[8,9], substantial changes in regional hydroclimate might be expected. However, such regional-scale changes are implicitly more uncertain[52,53] than broader-scale trends, particularly in light of limited observations and substantial (natural) variability that could alias anthropogenic trends. Trends in temperature, OHC, salinity, precipitation and evaporation observed in the Indian Ocean (including the IPWP) region over the common period of 1982–2012 are now discussed.

Spatial trends since the 1980s. Regional trend patterns across the broader Indian Ocean basin reveal changes in the heat and freshwater balance, with substantial sub-basin-scale features (FIG. 2). Global sea level rise, primarily caused by thermal expansion of the ocean (associated with the rise of global mean temperatures) and by mass addition (from increasing melt of glaciers, ice sheets, ice shelves), results in an overall increase of SSH over much of the IPWP (FIG. 2a), broadly consistent with that of SST (FIG. 2e), as both are affected by the rise of global mean temperature and sea level, as well as by the IPO.

Both remote and local SST anomalies, along with wind and ocean circulation, could induce changes in the freshwater balance over the Indian Ocean. Overall, SST exhibits marked warming over the entire Indian Ocean and within the MC (FIG. 2e), yet, no uniform precipitation increase across the basin is observed (FIG. 2d). For example, in the subtropical western Indian Ocean north-east of Madagascar and in the Arabian Sea, both SST and precipitation increased, as would be expected in a warming world. However, in the eastern Indian Ocean and the western MC, a consistent relationship between warming SST and increased precipitation is absent. Precipitation deficits (FIG. 2d) and enhanced evaporation (FIG. 2b) occurred in the region stretching from Sumatra west to 60°E, where freshwater fluxes from the ocean to the atmosphere were found during boreal summer averaged for the twentieth century[86] and exceeding 0.5 mm per day per year from 1979 to 2016 (REF.[81]).

Regional differences are also evident in SSS trends, suggesting a response to evaporation and precipitation but also additional influences from ocean circulation and dynamics. Clear freshening trends are evident in the north-east Bay of Bengal and north-eastern Arabian Sea, as well as in the south-east Indian Ocean, since the 1980s (FIG. 2f). The precipitation trends in both of the northern Indian Ocean marginal seas indicate increasing trends over the past few decades[81] (FIG. 2d), and, in the Bay of Bengal, this increase might also translate into increased freshening from river runoff.

Substantial SSS salinification trends occur to the east of Sri Lanka and along the west coast of Sumatra, stretching westward along the equator (FIG. 2f). This salinification is largely consistent with the declining trend in precipitation and enhanced evaporation[81] (FIG. 2b,d), although the spatial patterns in SSS, evaporation and precipitation along the equator and in the western Indian Ocean do not exactly coincide. It is likely that ocean dynamics and circulation contribute to the mismatch in scales, as does seasonality. For example, the underlying saltier water found at depth along the equator and west of Sumatra could have been upwelled in response to changes in wind stress and/or upwelling Kelvin waves that impact these regions[41]. Intriguingly, the salty SSS east of Sri Lanka (FIG. 2f) corresponds to the location of the Sri Lanka Dome, a seasonal cyclonic eddy that occurs in response to a local cyclonic wind stress curl pattern during the south-west monsoon that entrains saltier water entering from the Arabian Sea[87,88]. Changes in the strength or persistence of this feature could be responsible for the observed SSS trends.

In the subsurface, contrasting salinity trends in the Indo-Pacific warm-fresh pool have been observed with a salinification in the south-western Pacific Ocean and a freshening in the south-eastern tropical Indian Ocean since the 1980s[22,23,89] (FIG. 2f,h). Argo data over the period 2004–2013 revealed a comparable robust increase in salinity over the upper 100–150 m in the equatorial western Pacific but a freshening in the Indian Ocean over a similar depth range[23,89,90]. Although there are no direct measurements of the salt flux from within the MC, the sharp freshening coincides with where the ITF exits into the south-east Indian Ocean (FIG. 2f,h). The stronger ITF in the twenty-first century resulted in an enhanced transfer of warm, fresh water into the Indian Ocean

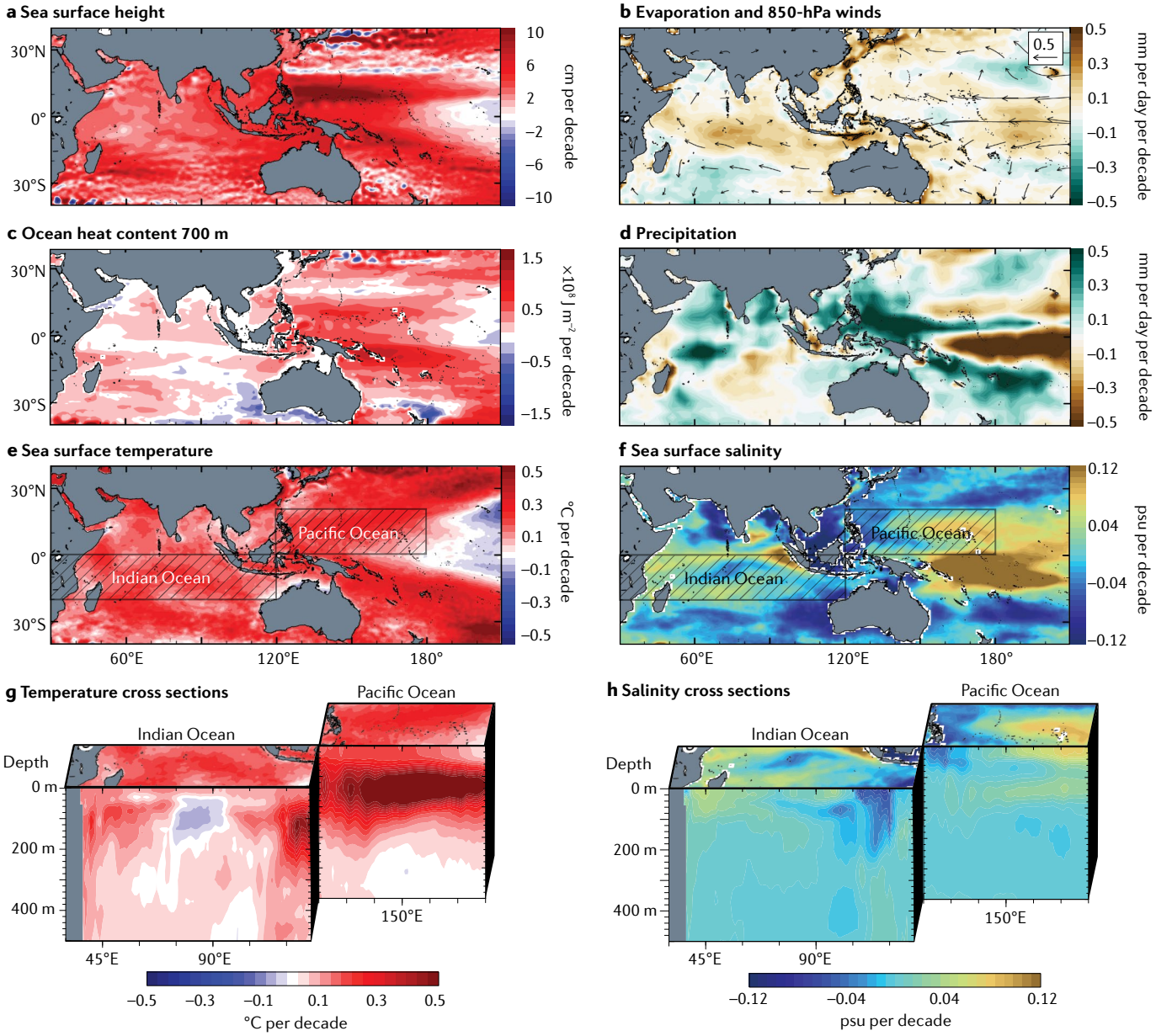

Fig. 2 | **Indo-Pacific trends.** Linear trends in sea surface height[171] (panel **a**), evaporation[172] and 850-hPa winds[173] (panel **b**), ocean heat content[174] in the upper 700 m (panel **c**), precipitation[175] (panel **d**), sea surface temperature[170] (panel **e**) and sea surface salinity[174] (panel **f**), and for cross sections of the upper 500 m of the Indian and Pacific oceans for temperature (panel **g**) and salinity (panel **h**). All trends are calculated over 1982–2012, except in panel **a**, which are calculated over 1992–2012. Subsurface data[174] in panels **g** and **h** are averaged meridionally over 0–20°S and 0–20°N, respectively. See Supplementary Table 1 for further details on data sets.

(FIG. 2g,h). A local maximum of ~0.5×10^8 J m^{-2} per decade in the upper 700 m OHC (OHC700) trend occurs in the south-east Indian Ocean, which appears to be linked to the MC and upstream to the Pacific (FIG. 2c).

Trends over the IPWP since the 1980s. Given the crucial role of the IPWP in the regional and global freshwater balance[91,92], changes in the broader MC region that represents the core of the IPWP (90°–150°E, 20°S–20°N; FIG. 1a) are further elucidated since 1950 (FIG. 3).

As has occurred in other parts of the global ocean[93], SST in the IPWP increased by ~0.5 °C since the 1950s (FIG. 3a), with the rate of warming increasing during the positive phase of the IPO from the 1980s to the mid-1990s (Supplementary Table 2). During this positive IPO phase, a concurrent increase in evaporation also occurred (FIG. 3e), but there appears to be little change in precipitation (FIG. 3f). During the negative phase of the IPO from 2002 to 2010, in contrast, marked negative evaporation–precipitation trends of over 2 mm per day per decade occurred in the MC, reflecting a freshwater flux from the atmosphere to the ocean[23]. The freshwater flux, in turn, lowered the upper ocean salinity (FIG. 3g), increasing OHC700 (FIG. 3b) and SSH (FIG. 3c), with subsequent impacts on the south-east Indian Ocean[23,40]. After 2012, the IPO index plateaued somewhat, reflecting a

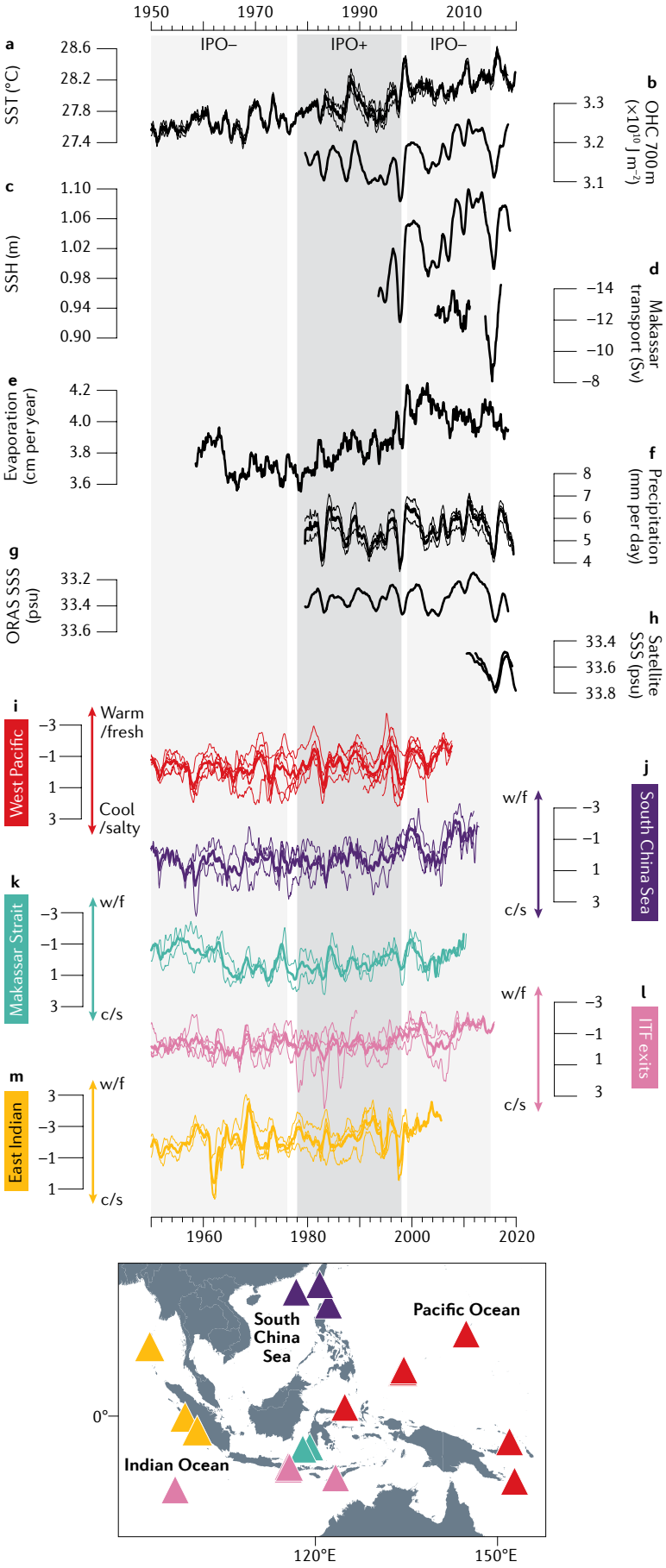

Fig. 3 | **Time series of key heat and freshwater metrics in the Indo-Pacific warm pool.** Observational and reanalysis time series from 1950–2020 for sea surface temperature (SST)[170,176,177] (panel **a**), ocean heat content (OHC)[174] in the upper 700 m (panel **b**), sea surface height (SSH)[171] (panel **c**), Indonesian throughflow (ITF) transport[101] in Makassar Strait (0–740 m depth range; panel **d**), evaporation[172] (panel **e**), precipitation[168,175,178] (panel **f**), sea surface salinity (SSS)[174] (panel **g**), satellite SSS[169,179] (panel **h**) and coral $\delta^{18}O$ *z*-scores grouped by region (see inset) for the west Pacific Ocean[126,131–134] (panel **i**), South China Sea[127,136,180] (panel **j**), Makassar Strait[137,138] (panel **k**), ITF exit regions[124,139–141] (panel **l**) and eastern Indian Ocean[12,15,181–183] (panel **m**). The seasonal cycle has been removed and smoothing applied for all panels (see Supplementary Information), with thin and thick lines illustrating individual and averaged time series, respectively. In panels **a**–**c** and **e**–**h**, observational and reanalysis products are spatially averaged over the region 90°–150°E, 20°S–20°N (FIG. 1a). In panel **d**, negative transport is into the Indian Ocean. Note inverted *y*-axes in panels **d**, **g** and **h**. Dark grey and light grey shading indicates positive and negative phases of the Interdecadal Pacific oscillation (IPO)[184,185]. See Supplementary Tables 1,3 for details on individual time series.

pause or reversal of the strengthening tropical Pacific trade winds. This pause acted to subdue the trends in SST, SSH and OHC700 within the MC (FIG. 3a–c).

The ITF strongly contributes to the salinity trends observed in the IPWP and the south-east Indian Ocean[94], and also influences observed trends in temperature stratification[95–97], SSH[22] and OHC[10,11,78,82,98–100]. The longest direct time series of velocity and transport of the ITF in the inflow passage of Makassar Strait reveals marked interannual variability since ~2008 (REF.[101]) (FIG. 3d). For example, Makassar Strait throughflow decreased during the 2014–2016 El Niño (FIG. 3d), with accompanying lower SSH and OHC700 (FIG. 3b,c) in the IPWP. The Pacific trade winds relaxed during the 2014–2016 El Niño event, acting to decrease the sea level in the western Pacific, while a concurrent negative IOD event raised the sea level in the Indian Ocean. The resultant changes combined to reduce the pressure gradient between the Pacific and Indian oceans that drives the ITF[37,102]. In addition, during El Niño events, the passage of buoyant freshwater through the South China Sea changes to be via the eastern pathway, introducing a freshwater 'plug' at the entrance way into the Indonesian seas that diminishes the surface contribution of the ITF[39]. Conversely, with the return to La Niña conditions beginning in mid-2016 through 2017, the Makassar Strait throughflow increased to a record high of >14 Sv, with corresponding changes in SSH, OHC700, precipitation and SSS (FIG. 3).

The geostrophic transport measured over the period 1984–2013 across the long-running IX1 expendable bathythermograph transect — where the ITF exits into the south-east Indian Ocean (FIG. 1b) — reveals strengthening of about 1 Sv per decade (REFS[103,104]). However, it remains unclear whether an increased volume transport translates to increased heat transport, given differences in the vertical profiles of heat and velocity[35,98,105]. Furthermore, the total integrated transport (FIG. 3d) obscures extensive changes in the depth and strength of the velocity maximum in the transport profile that

Geostrophic
Resulting from a balance between pressure gradients and the Coriolis force.

Pycnocline
Layer in the ocean in which water density increases rapidly with depth.

have occurred[101]. Accurate quantification of the freshwater and heat exchange between the Pacific and Indian oceans requires direct measurements of the thermal and haline profiles, in addition to the ITF transport profile.

Strong year-to-year variability coupled with limited observational records within the IPWP make it difficult to determine if longer-term trends exist in the region. Indeed, while basin-wide SST has warmed during the past 30 years, trends in precipitation, SSS and subsurface properties indicate greater regional variability. This regional variability confounds the ability to unequivocally state whether there has been a commensurate long-term intensification of the hydrological cycle or heat balance in the Indian Ocean. Thus, local SST changes might have little effect on the hydrological cycle[42], suggesting that the effect of regional ocean dynamics could dominate at the timescales considered.

The IPO oceanic connection. Multi-decadal Pacific variability associated with the IPO can affect heat and freshwater changes in the broader Indian Ocean region through an atmospheric and oceanic teleconnection, the latter of which is now discussed.

The pattern of SSH trends in the IPWP and the Indian Ocean basin reflect the combined effects of global sea level rise and the IPO[106–112]. The IPO induces the horseshoe pattern on the Pacific side of the IPWP (FIG. 4), which intensifies the SSH changes in the western tropical Pacific relative to the background SSH in the entire IPWP domain (FIG. 2a). Changes in SSH in the western tropical Pacific are transmitted through the Indonesian seas via coastal Kelvin waves, impacting SSH in the IPWP and south-east tropical Indian Ocean. This process operates on interannual to multi-decadal timescales[36,113,114] and reflects the linkage of upper-ocean steric height signals (primarily in the pycnocline) throughout the IPWP. The signals include both a thermosteric (FIG. 2g) and halosteric contribution (FIG. 2h), such that both warming and freshening can contribute to the steric height changes across the region (FIG. 2a).

In the mean, the Indo-Pacific pressure gradient is mainly driven by the large-scale wind field and the thermosteric component of steric height. However, the halosteric-driven pressure gradient is particularly important for regulating interannual and long-term ITF variability[40]. Indeed, the regional water cycle of the MC has proven to be critical in regulating both the ITF strength (via changes to the halosteric pressure gradient) and the vertical structure (via formation of buoyant surface pools that impede surface transport)[23,39,92], with impacts for the oceanic circulation, MC water properties and the downstream Indian Ocean[23,40,46,90,94]. For example, fed by the large salinity-driven signal in the MC and ITF exit region, the Leeuwin Current strengthened by 30% in austral summer 2010–2011, contributing to an extensive marine heatwave off Western Australia[21].

The change of the IPO index from predominantly positive to negative values from the 1990s to 2000s, associated with an observed strengthening of the Walker circulation and the tropical Pacific trade winds[67,68], caused dramatic changes in the IPWP region as a result of a strengthened ITF (FIG. 4e). The increased ITF during this hiatus period (2000–2010) led to a marked OHC increase in the main thermocline (100–350 m) of the Indian Ocean[10,11,78,83]. Enhanced precipitation over the IPWP during the hiatus also acted to strengthen the advection of freshwater anomalies within the ITF[23,89]. The largest OHC and salinity anomalies were mainly confined to the south-east Indian Ocean[22,23,89,96] (FIGS 2c,g,h,4). Models suggest that it might take around a decade for the ITF waters to completely traverse across the Indian Ocean[115], explaining why the thermal and haline changes were not as pronounced in the central and western tropical Indian Ocean basin. In addition, the locally wind-forced upwelling[85,116] combined with Rossby wave propagation from the eastern boundary[117] together can act to control the zonal propagation of the ITF influence into the central and western Indian Ocean[118].

The IPO atmospheric connection. The atmospheric teleconnection is also important. The reversals in near-surface salinity trends observed in the western Pacific are also driven by intensification of the Walker circulation associated with the strengthened Pacific trade winds during the negative IPO phase that substantially enhanced the precipitation over the MC, at the expense of that in the Pacific[23,89] (FIG. 4). Composites further reveal increasing summertime precipitation trends in the Bay of Bengal and the eastern Arabian Sea during 1996–2016 (IPO negative) compared with 1979–1997 (IPO positive)[81]. Using a moisture budget approach, 51% of the increased evaporation–precipitation trends can be attributed to enhanced dynamic divergence in the central eastern Indian Ocean associated with the westward shift of the Walker circulation[81] (FIG. 4). In the south-western Indian Ocean, 34% of the enhanced moisture supply can be linked to a stronger dynamic advection in response to the land–sea thermal contrast.

The atmospheric teleconnection from the Pacific Ocean to Indian Ocean can also induce OHC changes within the Indian Ocean basin. Decadal western Indian Ocean OHC variations primarily arise from oceanic Rossby waves triggered by anomalous wind stress curl and Ekman pumping in the central Indian Ocean, itself induced by a remote atmospheric response to Pacific IPO forcing through the zonal Walker circulation[85,119,120]. As such, both remote Pacific winds and local wind forcing from within the Indian Ocean basin influence regional heat and freshwater balance, though their spatial footprint differs. In the eastern Indian Ocean, conditions are more directly affected by Pacific winds, while the western Indian Ocean region is more affected by local winds[85] that can generate upwelling that impacts the thermocline and brings up saltier water from below[100,119,120] (FIGS 2,4).

IPO-related changes in the Walker circulation and wind forcing can modulate OHC changes via both the oceanic and the atmospheric bridge[120], contributing to the observed changes discussed earlier in this section: for the oceanic pathway, equatorial Pacific wind forcing results in western Pacific OHC and thermocline variations, affecting ITF transport, which are then transmitted through the MC to the eastern Indian Ocean. For the atmospheric pathway, local IPO-driven wind forcing over the Indian Ocean generates Ekman pumping

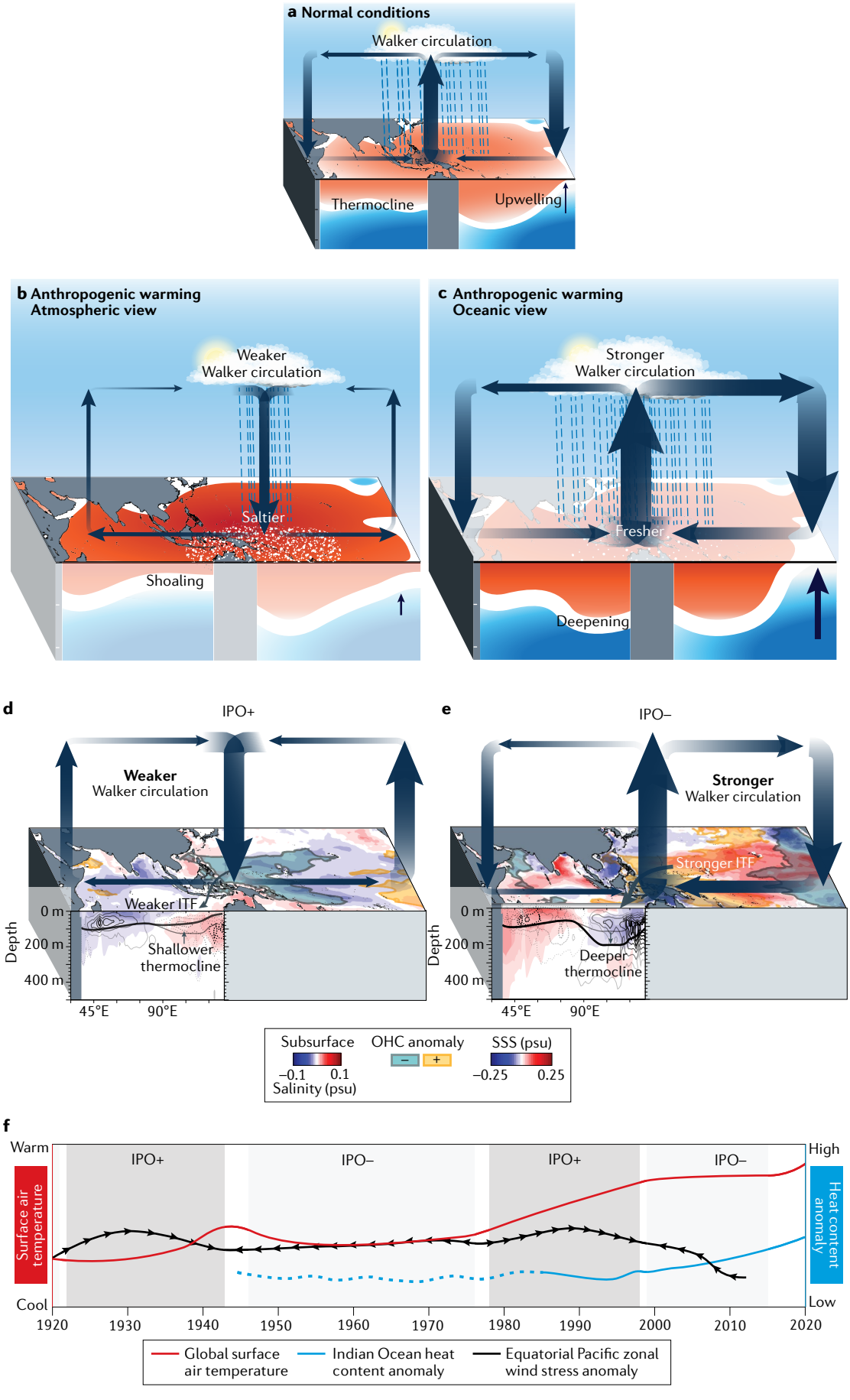
a Normal conditions
Walker circulation
Thermocline
Upwelling
b Anthropogenic warming
Atmospheric view
Weaker
Walker circulation
Saltier
Shoaling
c Anthropogenic warming
Oceanic view
Stronger
Walker circulation
Fresher
Deepening
d
IPO+
Weaker
Walker circulation
Weaker ITF
Shallower
thermocline
Depth
0 m
200 m
400 m
45°E
90°E
e
IPO–
Stronger
Walker circulation
Stronger ITF
Deeper
thermocline
Subsurface
OHC anomaly
SSS (psu)
–0.1
0.1
Salinity (psu)
–0.25
0.25
f
Warm
Cool
IPO+
IPO–
IPO+
IPO–
High
Low
Surface air temperature
Heat content anomaly
1920
1930
1940
1950
1960
1970
1980
1990
2000
2010
2020
Global surface air temperature
Indian Ocean heat content anomaly
Equatorial Pacific zonal wind stress anomaly

◀ Fig. 4 | **Impacts of anthropogenic warming and multi-decadal variability associated with the Interdecadal Pacific oscillation on Indo-Pacific climate.** Mean climatological Indo-Pacific climate conditions (panel **a**) and expected changes in a warming world from an atmospheric (panel **b**) and an oceanic (panel **c**) perspective. Salinity, temperature, upper 700 m ocean heat content (OHC) and thermocline anomalies during positive Interdecadal Pacific oscillation (IPO) phases, when the Walker circulation and Indonesian throughflow (ITF) are weaker (panel **d**), and during negative IPO phases, when the Walker circulation and ITF are stronger (panel **e**). Positive and negative subsurface temperature changes are indicated by solid and dashed contours, respectively, drawn at 0.1 °C intervals. Idealized time series of global surface air temperature, equatorial Pacific zonal wind stress anomaly (with arrows indicating easterly or westerly anomaly) and Indian Ocean upper 700 m OHC anomaly (panel **f**), highlighting warming surge and slowdown periods during positive and negative IPO phases. SSS, sea surface salinity.

in the central Indian Ocean that results in thermocline adjustments in the west[85].

Long-term context

Given substantial multi-decadal variability of the Indo-Pacific climate system, contemporary heat and freshwater changes need to be put into a longer-term context to aid the attribution of Indian Ocean trends to anthropogenic versus natural forcing. Continuous, multi-century records of hydrologic and thermal variability from coral climate archives (BOX 1) provide a long-term context for tropical ocean regions, where in situ observations often only extend a few decades.

Centennial trends. While the lengths of the coral records vary, the majority of Indian Ocean[121] and IPWP (FIG. 3) corals indicate warming and freshening since the 1980s, consistent with instrumental records. Moreover, compared with the second half of the twentieth century, individual IPWP coral records that extend back to the 1800s are consistently characterized by cooler and saltier conditions (FIG. 5). Multi-century reconstructions of tropical Indian Ocean and tropical western Pacific SST from a network of corals further indicate that the tropical Indo-Pacific Ocean gradually cooled until modern industrial-era warming began around the mid-nineteenth century[121,122]. Since 1850, coral-based reconstructions estimated that the average rate of warming across the tropical Indian Ocean has been 0.04 °C per decade, and, in the western Pacific, 0.03 °C per decade[121].

Yet, warming and freshening has not occurred at a uniform rate everywhere across the IPWP or within the tropical Indian Ocean. In general, contemporary and long-term trends in coral $\delta^{18}O$ are strongest in the western Pacific Ocean, decreasing in magnitude along the pathway of the ITF to lowest trends in the tropical eastern Indian Ocean (Supplementary Table 4). In addition, warming and freshening of the tropical south-east Indian Ocean is reduced compared with other parts of the tropical Indian Ocean[123] (FIG. 5). These differences have been attributed to an increase in seasonal upwelling in the eastern Indian Ocean, resulting in the tropical Indian Ocean trending towards a more positive IOD-like mean state[123]. More generally, however, long-term coral $\delta^{18}O$ (combined freshening and warming signal) and $\delta^{18}O_{sw}$ (freshening signal) trends across the Indo-Pacific have been attributed to an intensification of the hydrologic cycle[124–127], supporting multi-model projections[128].

Spatial patterns. The location of coral $\delta^{18}O$ samples along the pathways of oceanic exchange that connect the Indo-Pacific also offer unique long-term insights into the interactions and influences of interannual and decadal climate phenomena that are difficult to ascertain using coarsely resolved models, short observational data sets and sparse in situ and simulated $\delta^{18}O_{sw}$ data (FIGS 3,5). For instance, a strong negative excursion in coral $\delta^{18}O$ in the western Pacific records in the year 2000 (FIG. 3i) not only coincides with excursions in SSS (FIG. 3g,h), precipitation (FIG. 3f), SSH (FIG. 3c), OHC (FIG. 3b) and, to a lesser extent, SST (FIG. 3a) and evaporation (FIG. 3e) but also appears in some coral regions, such as the ITF exit region, where the excursion is evident in ~2002 (FIG. 3l). While not all excursions are as evident at all sites, it is clear that the full coral network must be utilized in synthesis with ocean and climate models to understand Indo-Pacific oceanic exchange and the underlying climate drivers, their interactions and their non-stationarity.

The network of palaeoclimate coral time series across the IPWP reveal spatial variability in dominant drivers of climate variability. In the western Pacific, interannual variability (namely, ENSO-driven advection) dominates thermal and hydrological variability for the past several hundred years[126,129–134] (FIGS 3,5). However, for coral records in the MC and eastern Indian Ocean, more complex and non-stationary combinations of interannual to multi-decadal variability (ENSO, IOD and IPO) emerge. At the Luzon Strait entrance to the South China Sea, for instance, strong influences of ENSO, as well as the IPO, alter the strength of the Kuroshio intrusion over the nineteenth and twentieth centuries[127,135,136] (FIG. 3j). Farther downstream in the southern Makassar Strait (FIG. 3k), influences of ENSO are also evident over the nineteenth and twentieth centuries[137–139]. Here, however, the impact of the IPO with its characteristic ENSO-type spatial pattern is inconsistent, likely owing to non-stationary climate interactions that become more apparent on longer timescales.

Coral sites within and immediately downstream of the main ITF exit passages (Lombok Strait and Timor Passage; FIG. 3) resolve a combination of Pacific decadal variability, ENSO, IOD and monsoon influences[124,139–141]. At Cocos Keeling (12.16°S, 96.87°E), for example, enhanced ITF transport during negative IPO intervals results in fresher surface ocean conditions[141], suggesting an important role of Pacific decadal variability in influencing ITF strength. Notably, this mechanism could also explain the modulation of tropical Indian Ocean warming rates that contributed to global warming slowdowns or accelerations over the past two centuries[141]. Such processes are consistent with inferences made from observational data on the role of decadal variations in Pacific trade wind strength in modulating ITF transport and, in turn, altering the spatial pattern of Indian Ocean surface warming trends[82]. Coral compilations further indicate that the magnitude of decadal variability was stronger in the tropical Indian Ocean during the late nineteenth century compared with the twentieth century, suggesting that the modern instrumental record might not fully estimate the effects of the IPO in the Indian Ocean, given the short (~15-year) extent of observations.

$\delta^{18}O$
Oxygen isotope composition in 'delta' notation, referring to relative departure of sample oxygen isotopic ratios $^{18}O/^{16}O$ compared with a standard. Coral calcium carbonate $\delta^{18}O$ reflects combined sea surface temperature and seawater $\delta^{18}O$ influences.

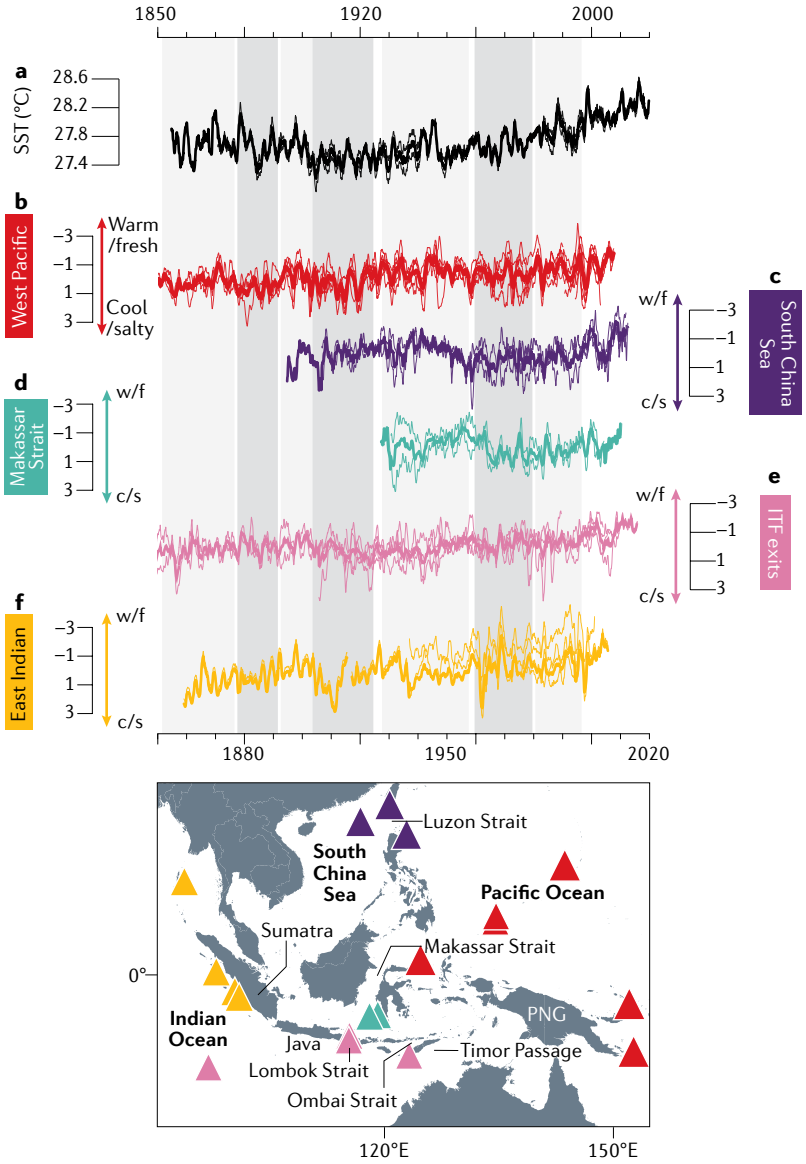

Fig. 5 | **Time series of sea surface temperature and coral proxy reconstructions over the Indo-Pacific warm pool.** Time series for the period 1850–2020 of sea surface temperature (SST)[170,176,177] (panel **a**) and coral $\delta^{18}O$ z-scores grouped by region (see inset) for the west Pacific Ocean[126,131–134] (panel **b**), South China Sea[127,136,180] (panel **c**), Makassar Strait[137,138] (panel **d**), Indonesian throughflow (ITF) exit regions[129,139–141] (panel **e**) and eastern Indian Ocean[12,15,181–183] (panel **f**). The SST products in panel **a** are spatially averaged over the region 90°–150°E, 20°S–20°N (FIG. 1a). The seasonal cycle has been removed and smoothing applied for all time series (see Supplementary Information), with thin and thick lines illustrating individual and averaged time series, respectively. Dark grey and light grey shading indicate positive and negative phases of the Interdecadal Pacific oscillation[184,185], respectively. See Supplementary Tables 1,3 for further details on individual time series. PNG, Papua New Guinea.

In the eastern Indian Ocean, corals from the upwelling region instead more clearly resolve the IOD, making it possible to reconstruct IOD variability to better understand its interactions with ENSO and the IPO. These IOD reconstructions are critical, given that sparse, modern in situ data have such a limited temporal record for the examination of IOD–ENSO interactions and their non-stationarity, causing considerable debate throughout the climate community[142–145]. Multiple centuries of reconstructed IOD variability indicate that positive IOD events have become more frequent and intense since the 1960s[12,15], and will imminently move outside of the range of pre-industrial variability if current trends continue[123]. Reconstructions of twentieth century IOD variability from the tropical Indian Ocean reveal that the strength of the year-to-year relationship between the IOD and ENSO has varied[12,124,146], and that this interaction is strongest when ENSO variability itself is strong[12]. A longer perspective over the last millennium further demonstrates a tight and persistent coupling between the magnitude of IOD and ENSO variability, highlighting the importance of the interactions between these two climate phenomena in shared Indo-Pacific climate variability[15,123]. At multi-decadal timescales, a comparison of CESM1-LME model simulations, observational data and the last millennium coral reconstruction additionally indicate that the IPO modulates positive IOD event recurrence[15], with thermocline depth variability in the eastern equatorial Indian Ocean having an important impact in preconditioning the development of positive IOD events[20,99].

Implications for contemporary changes. Owing to the importance of constraining past behaviour to give context to contemporary and future changes, coral-based reconstructions of SST and the hydrological cycle are common.

Indo-Pacific variability over the nineteenth and twentieth centuries from coral reconstructions indicates long-term freshening and warming trends throughout the region that vary in magnitude between the western Pacific Ocean, eastern Indian Ocean and western Indian Ocean[121–123]. At the same time, Indo-Pacific coral records resolve strong interannual to multi-decadal variability that is driven by spatially and temporally shifting interactions between ENSO, the IPO and the IOD as signals propagate to the Indian Ocean via the ITF and, more broadly, the MC oceanic bridge. Untangling past changes in these spatiotemporal interactions will require expanded regional proxy syntheses and proxy–model comparisons, which, together, have the potential to provide critical long-term hydroclimate perspectives and context for the observational and remote sensing data sets of the last 20–30 years, as well as future projections from climate models.

Summary and future perspectives

At the basin scale, the Indian Ocean has warmed throughout the twentieth century, the trends of which can be unequivocally attributed to human-induced climate change. At regional and short temporal timescales, however, there is inconclusive evidence about whether contemporary warming and freshening trends observed in the eastern Indian Ocean and the MC region are a result of anthropogenic forcing. Instead, observed heat and freshwater changes since 1980 likely result from IPO phasing (specifically, the negative phase of the IPO since the 2000s), as reflected in changes of the Walker circulation, and the resultant footprints in precipitation, SSS, OHC, SSH and ITF transport (FIG. 4).

To be able to unequivocally detect and attribute further anthropogenic change in the Indian Ocean's

heat and freshwater balance at a regional scale — of importance for climate risk assessments for vulnerable societies in Indian Ocean rim countries — many key questions need resolving.

On long timescales, warming trends appear to increasingly dominate OHC variability in the global ocean, compared with the contribution from multi-decadal variability on regional scales, such as associated with the IPO[147]. Yet, the adequacy of sufficient ocean observations for attribution of regional heat and freshwater trend estimates remains suboptimal in many areas of the world ocean[148]. In addition to the relatively short record that can be affected by the residual of interannual variability that is filtered out of the trends, the fidelities of some data sets also pose a challenge in providing accurate quantification of the trends. These include the uncertainties of the evaporation estimates from OAFlux (in fact, for all evaporation estimates[149]) and the uncertainties of ORAS4 in representing salinity in regions and periods when there is a lack of observations (within the MC or prior to the Argo period).

The case for detecting and attributing trends in the oceanic water cycle is even more complex, whether considering the aliasing by the IPO or trends arising from anthropogenic forcing. For example, it remains unclear whether the freshening in the MC and the eastern Indian Ocean is caused by an enhancement of local precipitation, enhanced advective freshwater flux through the ITF or both. Even if the cause is advective freshwater flux, it is unclear whether it reflects a transport signal or freshwater input; that is, if the ITF is transporting more or less freshwater, is that because water sources are becoming fresher or saltier, or because there is an increase or decrease in the overall ITF transport? These specific issues and questions motivate future effort to address higher-level science questions associated with the emergence of anthropogenic signals in IPWP subregions and the relative contributions of atmospheric and oceanic drivers to multi-decadal change in the IPWP.

However, addressing these research questions is challenged by several factors in the broader Indian Ocean region, including the sparsity of high-quality in situ observations for validating satellite SSS and the differences in the sampling scales between satellite SSS with 40–150-km footprints and in situ pointwise measurements. Furthermore, a lack of systematic measurements of (sub)surface salinity in the MC hamper quantifying freshwater transport by the ITF and its change. Hence, maintaining and expanding the current observing systems, both of remote sensing and in situ observations, will be crucial. Understanding the vertical profiles of transport and properties of the ITF and how they change in response to wind and buoyancy forcing is a key consideration for their subsequent impact on the heat and freshwater balance in the Indian Ocean[36,98]. ITF velocity profile measurements in particular will help address uncertainties in heat and freshwater transport through the Indonesian seas and its variability over time.

For remote sensing efforts, satellite SSS resolution, continuity and calibration across continuity missions are critical factors influencing the capability to study ocean-water cycle linkages in the IPWP region. Indeed, while the SMAP and SMOS data have provided relatively consistent characterization of SSS variability in the MC and Indian Ocean region[92], the continuity of satellite SSS beyond these missions is not ensured. Observations of in situ SSS need to be enhanced, especially in the MC region, as they are essential for satellite SSS validation. In the ITF exit region and within the MC with its complex topography, substantial benefits could be realized from improved coastal altimetry[150] to refine estimates of the anomalies of surface geostrophic flow and the mean dynamic topography used for obtaining the time-mean surface geostrophic flow[151–153].

The combined use of observations with model simulations is considered the most viable method to separate the forced signal from noise and ascertain primary drivers of variability and change[148]. Yet, the presence of spurious model drift at present often complicates the detection of real trends[154]. Hence, improvements are also needed for resolution and parameterizations of climate models to more skilfully represent the MC region and the intricate heat and freshwater exchange between the Pacific Ocean and the Indian Ocean, and reduce spurious model drift in the heat and freshwater balance. Given the large tidal mixing in the MC region[41], the inclusion of a tidal mixing parameterization that is largely missing in most current-generation ocean reanalyses and climate models is critical for a realistic representation of the heat and salt flux at the ITF exit. A focused model intercomparison project for CMIP7 could harness community efforts towards these model improvements[155–158].

Another research question more fundamentally beckons as to how to link the 'short' observational records with interannual (ENSO, IOD) to multi-decadal climate phenomena (IPO), especially in light of a non-stationary climate that, in turn, likely leads to changing characteristics of these same climate modes. While coral proxy records provide a useful tool for addressing these types of questions, coral-based reconstructions can themselves also be challenged by the non-stationarity in the climate system. This Review highlights the utility of palaeo archives for extending records of heat and freshwater changes in data-sparse regions farther back in time. Yet, further efforts are required to better understand the underlying cause for, and to resolve discrepancies between, palaeo proxies and modern in situ observations in identifying relationships between climate modes that are non-stationary and/or that might vary across timescales, such as identified here for the MC region.

Fortunately, some of these efforts are already underway, for example, through the development of the Past Global Changes (PAGES) CoralHydro2k coral proxy database that will, in part, be used for regional reconstructions and syntheses. Alongside regional syntheses of existing coral records, expanding the network of coral proxy sites would help to improve the quality of early SST products[159,160], when direct observations from the Indian Ocean region were sparse. For example, the long-term trends in the IPWP from multiple coral $\delta^{18}O$ records during the 1800s do not match corresponding SST products derived from sparse observational data (FIG. 5), raising questions about the fidelity of early SST records[161]. Sparse in situ and simulated $\delta^{18}O_{sw}$

measurements through space and time similarly limit the utility of gridded $\delta^{18}O_{sw}$ products[162,163] in examining multi-decadal and long-term hydroclimatic variability. Expanded $\delta^{18}O_{sw}$ sampling and monitoring networks that operate alongside expanded observational networks would complement the continuing collection of other observational data, all of which is crucial for calibrating and validating coral palaeoclimate records. Overall, expanding the network of palaeo records and using them more widely for regional reconstructions can be of great benefit to complement our relatively short observational perspective.

Given the substantial interbasin heat and freshwater exchange from the Pacific Ocean to the Indian Ocean and the large changes seen in the MC region, a key outstanding question relates to the fate of the heat and freshwater within the Indian Ocean basin. Future coral syntheses provide opportunities to track the propagation of the ITF heat and freshwater signal into the central and western Indian Ocean. Modelling has shown that the ITF is a major contributor to the Agulhas Current[164], most likely via the South Equatorial Current[165], although it can take a decade for these waters to completely traverse the Indian Basin[115]. There are few observational studies that provide an unambiguous link from the ITF to the Agulhas and Atlantic: the ITF surface freshwater signal is traced to the Seychelles–Chagos Thermocline Ridge[118,166], as is the Indonesian Intermediate Water to around the same longitude[41]. The trail goes cold after that because of mixing with the salty Red Sea water and other water masses. Hence, as already flagged as a priority research area by the decadal review of the Indian Ocean Observing System (IndOOS)[8], maintenance of the tropical RAMA (Research Moored Array for African–Asian–Australian Monsoon Analysis and Prediction) array[167], the 32°S GO-SHIP hydrographic section and the expendable bathythermograph line across the Agulhas Current (FIG. 1) in the south-west Indian Ocean are crucial for closing the heat and freshwater budget of the Indian Ocean on multi-decadal timescales.

To address these outstanding challenges for quantifying change in the oceanic heat and freshwater balance in the Indian Ocean, as well as within the IPWP that represents a critical pivot in the global climate system, a multi-pronged approach is warranted that capitalizes on a systematic integration of in situ observations, remote sensing, numerical modelling efforts and palaeo proxy networks across temporal and spatial scales.

Published online: 20 July 2021

1. Schmitt, R. W. Salinity and the global water cycle. *Oceanography* **21**, 12–19 (2008).
2. Lagerloef, G., Schmitt, R., Schanze, J. & Kao, H.-Y. The ocean and the global water cycle. *Oceanography.* **23**, 82–93 (2010).
3. Gordon, A. L. The marine hydrological cycle: The ocean's floods and droughts. *Geophys. Res. Lett.* **43**, 7649–7652 (2016).
4. Huntington, T. G. Evidence for intensification of the global water cycle: Review and synthesis. *J. Hydrol.* **319**, 83–95 (2006).
5. Helm, K. P., Bindoff, N. L. & Church, J. A. Changes in the global hydrological-cycle inferred from ocean salinity. *Geophys. Res. Lett.* **37**, L18701 (2010).
6. Durack, P. J., Wijffels, S. E. & Matear, R. J. Ocean salinities reveal strong global water cycle intensification during 1950 to 2000. *Science* **336**, 455–458 (2012).
Demonstrates the intensification of the water cycle in the second half of the twentieth century based on ocean salinities in observations and climate model simulations.
7. Held, I. M. & Soden, B. J. Robust responses of the hydrological cycle to global warming. *J. Clim.* **19**, 5686–5699 (2006).
8. Beal, L. M. et al. A road map to IndOOS-2: Better observations of the rapidly warming Indian Ocean. *Bull. Am. Meteorol. Soc.* **101**, E1891–E1913 (2020).
Summary of the findings and recommendations of the decadal review of the Indian Ocean Observing System (IndOOS).
9. Han, W. et al. Indian Ocean decadal variability: a review. *Bull. Am. Meteorol. Soc.* **95**, 1679–1703 (2014).
Reviews the state of knowledge of decadal variability in the Indian Ocean from observations, reanalyses and climate model simulations.
10. Lee, S.-K. et al. Pacific origin of the abrupt increase in Indian Ocean heat content during the warming hiatus. *Nat. Geosci.* **8**, 445–450 (2015).
11. Nieves, V., Willis, J. K. & Patzert, W. C. Recent hiatus caused by decadal shift in Indo-Pacific heating. *Science* **349**, 532–535 (2015).
Demonstrates redistribution of upper ocean heat content between the Pacific and Indian oceans from observations during the global warming hiatus (1993–2012).
12. Abram, N. J., Gagan, M. K., Cole, J. E., Hantoro, W. S. & Mudelsee, M. Recent intensification of tropical climate variability in the Indian Ocean. *Nat. Geosci.* **1**, 849–853 (2008).
13. Cai, W., Cowan, T. & Sullivan, A. Recent unprecedented skewness towards positive Indian Ocean dipole occurrences and their impact on Australian rainfall. *Geophys. Res. Lett.* **36**, L11705 (2009).
14. Freund, M. B. et al. Higher frequency of Central Pacific El Niño events in recent decades relative to past centuries. *Nat. Geosci.* **12**, 450–455 (2019).
15. Abram, N. J. et al. Coupling of Indo-Pacific climate variability over the last millennium. *Nature* **579**, 385–392 (2020).
16. Cai, W. et al. Projected response of the Indian Ocean Dipole to greenhouse warming. *Nat. Geosci.* **6**, 999–1007 (2013).
17. Cai, W. et al. Increased frequency of extreme Indian Ocean Dipole events due to greenhouse warming. *Nature* **510**, 254–258 (2014).
18. Cai, W. et al. Increasing frequency of extreme El Niño events due to greenhouse warming. *Nat. Clim. Change* **4**, 111–116 (2014).
19. Annamalai, H., Potemra, J., Murtugudde, R. & McCreary, J. P. Effect of preconditioning on the extreme climate events in the tropical Indian Ocean. *J. Clim.* **18**, 3450–3469 (2005).
20. Ummenhofer, C. C., Biastoch, A. & Böning, C. W. Multidecadal Indian Ocean variability linked to the Pacific and implications for preconditioning Indian Ocean dipole events. *J. Clim.* **30**, 1739–1751 (2017).
21. Feng, M., Benthuysen, J., Zhang, N. & Slawinski, D. Freshening anomalies in the Indonesian throughflow and impacts on the Leeuwin Current during 2010–2011. *Geophys. Res. Lett.* **42**, 8555–8562 (2015).
22. Llovel, W. & Lee, T. Importance and origin of halosteric contribution to sea level change in the southeast Indian Ocean during 2005–2013. *Geophys. Res. Lett.* **42**, 1148–1157 (2015).
Highlights the importance of halosteric effects to observed twenty-first century sea level changes in the south-eastern Indian Ocean.
23. Hu, S. & Sprintall, J. Observed strengthening of interbasin exchange via the Indonesian seas due to rainfall intensification. *J. Geophys. Res.* **44**, 1448–1456 (2017).
Demonstrates how observed rainfall changes over the Maritime Continent contributed to an intensification of the Indonesian throughflow transport since the early 2000s.
24. Yu, L. Global variations in oceanic evaporation (1958–2005): The role of the changing wind speed. *J. Clim.* **20**, 5376–5390 (2007).
25. Pall, P. et al. Anthropogenic greenhouse gas contribution to flood risk in England and Wales in autumn 2000. *Nature* **470**, 382–385 (2011).
26. Lehmann, J., Coumou, D. & Frieler, K. Increased record-breaking precipitation events under global warming. *Clim. Change* **132**, 501–515 (2015).
27. Meredith, E. P., Semenov, V. A., Maraun, D., Park, W. & Chernokulsky, A. V. Crucial role of Black Sea warming in amplifying the 2012 Krymsk precipitation extreme. *Nat. Geosci.* **8**, 615–619 (2015).
28. Trenberth, K. E., Fasullo, J. T. & Shepherd, T. G. Attribution of climate extreme events. *Nat. Clim. Change* **5**, 725–730 (2015).
29. Ummenhofer, C. C. et al. How did ocean warming affect Australian rainfall extremes during the 2010/2011 La Niña event? *Geophys. Res. Lett.* **42**, 9942–9951 (2015).
30. Fowler, H. J. et al. Anthropogenic intensification of short-duration rainfall extremes. *Nat. Rev. Earth Environ.* **2**, 107–122 (2021).
31. Meehl, G. A. et al. Initialized Earth System prediction from subseasonal to decadal timescales. *Nat. Rev. Earth Environ.* **2**, 340–357 (2021).
32. Findell, K. L. et al. Rising temperatures increase importance of oceanic evaporation as a source for continental precipitation. *J. Clim.* **32**, 7713–7726 (2019).
33. Gimeno, L., Nieto, R. & Son, R. The growing importance of oceanic moisture sources for continental precipitation. *NPJ Clim. Atmos. Sci.* **3**, 27 (2020).
34. Schott, F. A., Xie, S.-P. & McCreary, J. Indian Ocean circulation and climate variability. *Rev. Geophys.* **47**, RG1002 (2009).
Reviews the state of knowledge of Indian Ocean circulation and climate variability across a range of timescales (seasonal, interannual and decadal).
35. Sprintall, J., Wijffels, S. E., Molcard, R. & Jaya, I. Direct estimates of the Indonesian Throughflow entering the Indian Ocean: 2004–2006. *J. Geophys. Res.* **114**, C07001 (2009).
36. Wijffels, S. E., Meyers, G. M. & Godfrey, J. S. A 20-yr average of the Indonesian Throughflow: Regional currents and the interbasin exchange. *J. Phys. Oceanogr.* **38**, 1965–1978 (2008).
37. Wyrtki, K. Indonesian through flow and the associated pressure gradient. *J. Geophys. Res.* **92**, 12941–12946 (1987).
38. Andersson, H. C. & Stigebrandt, A. Regulation of the Indonesian throughflow by baroclinic draining of the North Australian Basin. *Deep. Sea Res. I* **52**, 2214–2233 (2005).
39. Gordon, A. L. et al. South China Sea throughflow impact on the Indonesian throughflow. *Geophys. Res. Lett.* **39**, L11602 (2012).

40. Hu, S. & Sprintall, J. Interannual variability of the Indonesian Throughflow: The salinity effect. *J. Geophys. Res.* **121**, 2596–2615 (2016).
41. Sprintall, J. et al. Detecting change in the Indonesian seas. *Front. Marine Sci.* **6**, 257 (2019).
Reviews the current status of ocean observing systems and modelling to quantify changes in the heat and freshwater in the Indonesian seas and provides specific recommendations for observations needed to advance this goal.
42. Adler, R. F., Gu, G., Sapiano, M., Wang, J. J. & Huffman, G. J. Global precipitation: Means, variations and trends during the satellite era (1979–2014). *Surv. Geophys.* **38**, 679–699 (2017).
43. Yang, J., Liu, Q. & Liu, Z. Linking observations of the Asian monsoon to the Indian Ocean SST: Possible roles of Indian Ocean Basin mode and dipole mode. *J. Clim.* **23**, 5889–5902 (2010).
44. Sengupta, D., Raj, G. N. B. & Shenoi, S. S. C. Surface freshwater from Bay of Bengal runoff and Indonesian throughflow in the tropical Indian Ocean. *Geophys. Res. Lett.* **33**, L22609 (2006).
45. Mahadevan, A., Paluszkiewicz, T., Ravichandran, M., Sengupta, D. & Tandon, A. Introduction to the special issue on the Bay of Bengal: From monsoons to mixing. *Oceanogr.* **29**, 14–17 (2016).
46. Mahadevan, A. et al. Freshwater in the Bay of Bengal: Its fate and role in air-sea heat exchange. *Oceanogr.* **29**, 72–81 (2016).
47. Hu, S. et al. Interannual to decadal variability of upper-ocean salinity in the southern Indian Ocean and the role of the Indonesian throughflow. *J. Clim.* **32**, 6403–6421 (2019).
48. Gordon, A. L. Interocean exchange of thermocline water. *J. Geophys. Res.* **91**, 5037–5046 (1986).
49. Talley, L. D. & Sprintall, J. Deep expression of the Indonesian Throughflow: Indonesian intermediate water in the South Equatorial Current. *J. Geophys. Res.* **110**, C10009 (2005).
50. Zhai, P., Bower, A. S., Smethie, W. M. Jr & Pratt, L. J. Formation and spreading of Red Sea Outflow Water in the Red Sea. *J. Geophys. Res.* **120**, 6542–6563 (2015).
51. Bindoff, N. L. et al. in *Climate Change 2013: The Physical Science Basis. Contribution of Working Group I to the Fifth Assessment Report of the Intergovernmental Panel on Climate Change* Ch. 10 (eds Stocker, T. F. et al.) 867–952 (Cambridge Univ. Press, 2013).
52. Seager, R., Naik, N. & Vecchi, G. A. Thermodynamic and dynamic mechanisms for large-scale changes in the hydrological cycle in response to global warming. *J. Clim.* **23**, 4651–4668 (2010).
53. IPCC. in *Climate Change 2013: The Physical Science Basis. Contribution of Working Group I to the Fifth Assessment Report of the Intergovernmental Panel on Climate Change* (eds Stocker, T. F. et al.) 3–29 (Cambridge Univ. Press, 2013).
54. Smith, T. M., Arkin, P. A., Ren, L. & Shen, S. S. P. Improved reconstruction of global precipitation since 1900. *J. Atmos. Ocean. Technol.* **29**, 1505–1517 (2012).
55. DeAngelis, A. M., Qu, X., Zelinka, M. D. & Hall, A. An observational radiative constraint on hydrologic cycle intensification. *Nature* **528**, 249–253 (2015).
56. Xie, S.-P. et al. Global warming pattern formation: sea surface temperature and rainfall. *J. Clim.* **23**, 966–986 (2010).
57. Li, G., Xie, S.-P., Du, Y. & Luo, Y. Effects of excessive equatorial cold tongue bias on the projections of tropical Pacific climate change. Part I: The warming pattern in CMIP5 multi-model ensemble. *Clim. Dyn.* **47**, 3817–3831 (2016).
58. Cai, W. et al. Pantropical climate interactions. *Science* **363**, eaav4236 (2019).
59. Dong, L. & McPhaden, M. J. Why has the relationship between Indian and Pacific Ocean decadal variability changed in recent decades? *J. Clim.* **30**, 1971–1983 (2017).
60. Vecchi, G. A. et al. Weakening of tropical Pacific atmospheric circulation due to anthropogenic forcing. *Nature* **441**, 73–76 (2006).
61. Vecchi, G. A. & Soden, B. J. Global warming and the weakening of the tropical circulation. *J. Clim.* **20**, 4316–4340 (2007).
62. Newman, M. Winds of change. *Nat. Clim. Change* **3**, 538–539 (2013).
63. Deser, C., Phillisp, A. S. & Alexander, M. A. Twentieth century tropical sea surface temperature trends revisited. *Geophys. Res. Lett.* **37**, L10701 (2010).
64. Tokinaga, H., Xie, S.-P., Deser, C., Kosaka, Y. & Okumura, Y. M. Slowdown of the Walker circulation driven by tropical Indo-Pacific warming. *Nature* **491**, 439–443 (2012).
65. Roxy, M. K., Ritika, K., Terray, P. & Masson, S. The curious case of Indian Ocean warming. *J. Clim.* **27**, 8501–8509 (2014).
66. Cai, W., Sullivan, A. & Cowan, T. Shoaling of the off-equatorial south Indian Ocean thermocline: Is it driven by anthropogenic forcing? *Geophys. Res. Lett.* **35**, L12711 (2008).
67. L'Heureux, M., Lee, S. & Lyon, B. Recent multidecadal strengthening of the Walker circulation across the tropical Pacific. *Nat. Clim. Change* **3**, 571–576 (2013).
68. England, M. H. et al. Recent intensification of wind-driven circulation in the Pacific and the ongoing warming hiatus. *Nat. Clim. Change* **4**, 222–227 (2014).
69. Merrifield, M. A., Thompson, P. R. & Lander, M. Multidecadal sea level anomalies and trends in the western tropical Pacific. *Geophys. Res. Lett.* **39**, L13602 (2012).
70. Karnauskas, K. B., Seager, R., Kaplan, A., Kushnir, Y. & Cane, M. A. Observed strengthening of the zonal sea surface temperature gradient across the equatorial Pacific Ocean. *J. Clim.* **22**, 4316–4321 (2009).
71. Meng, Q. et al. Twentieth century Walker circulation change: data analysis and model experiments. *Clim. Dyn.* **38**, 1757–1773 (2012).
72. Solomon, A. & Newman, M. Reconciling disparate twentieth-century Indo-Pacific ocean temperature trends in the instrumental record. *Nat. Clim. Change* **2**, 691–699 (2012).
73. Seager, R. et al. Strengthening tropical Pacific zonal sea surface temperature gradient consistent with rising greenhouse gases. *Nat. Clim. Change* **9**, 517–522 (2019).
74. Zhang, L. et al. Indian Ocean warming trend reduces Pacific warming response to anthropogenic greenhouse gases: An interbasin thermostat mechanism. *Geophys. Res. Lett.* **46**, 10,882–10,890 (2019).
75. Heede, U. K., Fedorov, A. V. & Burls, N. J. Time scales and mechanisms for the tropical Pacific response to global warming: A tug of war between the ocean thermostat and weaker Walker. *J. Clim.* **33**, 6101–6118 (2020).
76. Medhaug, I. et al. Reconciling controversies about the 'global warming hiatus'. *Nature* **545**, 41–47 (2017).
77. Bindoff, N. L. et al. in *IPCC Special Report on the Ocean and Cryosphere in a Changing Climate* Ch. 5 (eds Pörtner, H.-O. et al.) 447–458 (Cambridge Univ. Press, 2019).
78. Feng, M. et al. The reversal of the multi-decadal trends of the equatorial Pacific easterly winds, and the Indonesian Throughflow and Leeuwin Current transports. *Geophys. Res. Lett.* **38**, L11604 (2011).
79. Vialard, J. Hiatus heat in the Indian Ocean. *Nat. Geosci.* **8**, 423–424 (2015).
80. Han, W. et al. Decadal variability of the Indian and Pacific Walker cells since the 1960s: Do they covary on decadal time scales? *J. Clim.* **30**, 8447–8468 (2017).
81. Han, Z., Su, T., Zhang, Q., Wen, Q. & Feng, G. Thermodynamic and dynamic effects of increased moisture sources over the tropical Indian Ocean in recent decades. *Clim. Dyn.* **53**, 7081–7096 (2019).
82. Dong, L. & McPhaden, M. J. Interhemispheric SST gradient trends in the Indian Ocean prior to and during the recent global warming hiatus? *J. Clim.* **29**, 9077–9095 (2016).
83. Liu, W., Xie, S.-P. & Lu, J. Tracking ocean heat uptake during the surface warming hiatus. *Nat. Commun.* **7**, 10926 (2016).
84. Li, Y. et al. Multidecadal changes of the upper Indian Ocean heat content during 1965–2016. *J. Clim.* **31**, 7863–7884 (2020).
85. Jin, X. et al. Influences of Pacific climate variability on decadal subsurface ocean heat content variations in the Indian Ocean. *J. Clim.* **31**, 4154–4174 (2018).
86. Ren, L., Arkin, P., Smith, T. M. & Shen, S. S. P. Global precipitation trends in 1900–2005 from a reconstruction and coupled model simulations. *J. Geophys. Res.* **118**, 1679–1689 (2013).
87. Vinayachandran, P. N. & Yamagata, T. Monsoon response of the sea around Sri Lanka: generation of thermal domes and anticyclonic vortices. *J. Phys. Oceanogr.* **28**, 1946–1960 (1997).
88. Burns, J. M. et al. On the dynamics of the Sri Lanka Dome in the Bay of Bengal. *J. Geophys. Res.* **122**, 7737–7750 (2017).
89. Du, Y. et al. Decadal trends of the upper ocean salinity in the tropical Indo-Pacific since mid-1990s. *Sci. Rep.* **5**, 16050 (2015).
90. Li, G. et al. Examining the salinity change in the upper Pacific Ocean during the Argo period. *Clim. Dyn.* **53**, 6055–6074 (2019).
91. Sprintall, J. et al. The Indonesian seas and their role in the coupled ocean–climate system. *Nat. Geosci.* **7**, 487–492 (2014).
92. Lee, T., Fournier, S., Gordon, A. L. & Sprintall, J. Maritime Continent water cycle regulates low-latitude chokepoint of global ocean circulation. *Nat. Commun.* **10**, 2103 (2019).
Using in situ and remotely sensed observations, demonstrates the importance of local contributions to the Maritime Continent freshwater balance on seasonal timescales and their implications for Indonesian throughflow transport.
93. Hartmann, D. L. et al. in *Climate Change 2013: The Physical Science Basis. Contribution of Working Group I to the Fifth Assessment Report of the Intergovernmental Panel on Climate Change* Ch. 2 (eds Stocker, T. F. et al.) 159–254 (Cambridge Univ. Press, 2013).
94. Phillips, H. E., Wijffels, S. E. & Feng, M. Interannual variability in the freshwater content of the Indonesian-Australian Basin. *Geophys. Res. Lett.* **32**, L03603 (2005).
95. Cheng, L. et al. Improved estimates of ocean heat content from 1960 to 2015. *Sci. Adv.* **3**, e1601545 (2017).
96. Li, Y., Han, W. & Zhang, L. Enhanced decadal warming of the southeast Indian Ocean during the recent global surface warming slowdown. *Geophys. Res. Lett.* **44**, 9876–9884 (2017).
97. Zhou, X., Alves, O., Marsland, S. J., Bi, D. & Hirst, A. C. Multi-decadal variations of the South Indian Ocean subsurface temperature influenced by Pacific Decadal Oscillation. *Tellus* **69**, 1308055 (2017).
98. Gruenburg, L. K. & Gordon, A. L. Variability in Makassar Strait heat flux and its effect on the eastern tropical Indian Ocean. *Oceanography* **31**, 80–87 (2018).
99. Zhang, L., Du, Y. & Cai, W. Low-frequency variability and the unusual Indian Ocean Dipole events in 2015 and 2016. *Geophys. Res. Lett.* **45**, 1040–1048 (2018).
100. Volkov, D. L., Lee, S.-K., Gordon, A. L. & Rudko, M. Unprecedented reduction and quick recovery of the South Indian Ocean heat content and sea level in 2014–2018. *Sci. Adv.* **6**, eabc1151 (2020).
101. Gordon, A. L. et al. Makassar Strait throughflow seasonal and interannual variability: An overview. *J. Geophys. Res.* **124**, 3724–3736 (2019).
102. Pujiana, K., McPhaden, M. J., Gordon, A. L. & Napitu, A. M. Unprecedented response of Indonesian throughflow to anomalous Indo-Pacific climatic forcing in 2016. *J. Geophys. Res.* **124**, 3737–3754 (2019).
103. Liu, Q.-Y., Feng, M., Wang, D. & Wijffels, S. Interannual variability of the Indonesian Throughflow transport: A revisit based on 30 year expendable bathythermograph data. *J. Geophys. Res.* **120**, 8270–8282 (2015).
104. Feng, M., Zhang, N., Liu, Q. & Wijffels, S. The Indonesian throughflow, its variability and centennial change. *Geosci. Lett.* **5**, 3 (2018).
105. Li, Y., Han, W., Wang, F., Zhang, L. & Duan, J. Vertical structure of the upper–Indian Ocean thermal variability. *J. Clim.* **33**, 7233–7253 (2020).
106. Hamlington, B. D., Leben, R. R., Strassburg, M. W., Nerem, R. S. & Kim, K.-Y. Contribution of the Pacific Decadal Oscillation to global mean sea level trends. *Geophys. Res. Lett.* **40**, 50950 (2013).
107. Hamlington, B. D. et al. Uncovering an anthropogenic sea-level rise signal in the Pacific Ocean. *Nat. Clim. Change* **4**, 782–785 (2014).
108. Palanisamy, H. et al. Regional sea level variability, total relative sea level rise and its impacts on islands and coastal zones of Indian Ocean over the last sixty years. *Glob. Planet. Change* **116**, 54–67 (2014).
109. Hamlington, B. D. et al. An ongoing shift in Pacific Ocean sea level. *J. Geophys. Res.* **121**, 5084–5097 (2016).
110. Deepa, J. S. et al. The tropical Indian Ocean decadal sea level response to the Pacific decadal oscillation forcing. *Clim. Dyn.* **52**, 5045–5058 (2019).
111. Jyoti, J., Swapna, P., Krishnan, R. & Naidu, C. V. Pacific modulation of accelerated south Indian Ocean sea level rise during the early 21st Century. *Clim. Dyn.* **53**, 4413–4432 (2019).
112. Gopika, S. J. et al. Aliasing of the Indian Ocean externally-forced warming spatial pattern by internal climate variability. *Clim. Dyn.* **54**, 1093–1111 (2020).

113. Lee, T. & McPhaden, M. J. Decadal phase change in large-scale sea level and winds in the Indo-Pacific region at the end of the 20th century. *Geophys. Res. Lett.* **35**, L01605 (2008).
114. Feng, M., McPhaden, M. J. & Lee, T. Decadal variability of the Pacific subtropical cells and their influence on the southeast Indian Ocean. *Geophys. Res. Lett.* **37**, L09606 (2010).
115. Song, Q., Gordon, A. L. & Visbeck, M. Spreading of the Indonesian throughflow in the Indian Ocean. *J. Phys. Oceanogr.* **34**, 772–792 (2004).
116. Tozuka, T., Yokoi, T. & Yamagata, T. A modeling study of interannual variations of the Seychelles Dome. *J. Geophys. Res.* **115**, C04005 (2010).
117. Birol, F. & Morrow, R. Source of the baroclinic waves in the southeast Indian Ocean. *J. Geophys. Res.* **106**, 9145–9160 (2001).
118. Gruenburg, L. K. *Indonesian Throughflow Heat Transport, and Spreading Within the Eastern Tropical Indian Ocean*. Doctoral thesis, Lamont-Doherty Earth Observatory, Columbia Univ. (2021).
119. Li, Y., Han, W., Hu, A., Meehl, G. A. & Wang, F. Multidecadal changes of the upper Indian Ocean heat content during 1965–2016. *J. Clim.* **31**, 7863–7884 (2018).
120. Ummenhofer, C. C. et al. Late 20th century Indian Ocean heat content gain masked by wind forcing. *Geophys. Res. Lett.* **47**, e2020GL088692 (2020).
Details the relative contribution of wind and buoyancy forcing for multi-decadal Indian Ocean heat content changes of the past 60 years, as well as spatial patterns and depth structure of upper-ocean temperature changes.
121. Tierney, J. E. et al. Tropical sea surface temperatures for the past four centuries reconstructed from coral archives. *Paleoceanography* **30**, 226–252 (2015).
122. Abram, N. J. et al. Early onset of industrial-era warming across the oceans and continents. *Nature* **536**, 411–418 (2016).
123. Abram, N. J. et al. Paleoclimate perspectives on the Indian Ocean Dipole. *Quat. Sci. Rev.* **237**, 106302 (2020).
Reviews the state of knowledge of the Indian Ocean Dipole from a palaeoclimatic perspective based on observations, proxies and climate model simulations.
124. Charles, C. D., Cobb, K., Moore, M. D. & Fairbanks, R. G. Monsoon–tropical ocean interaction in a network of coral records spanning the 20th century. *Mar. Geol.* **201**, 207–222 (2003).
125. Nurhati, I. S., Cobb, K. M. & Di Lorenzi, E. Decadal-scale SST and salinity variations in the central tropical Pacific: Signatures of natural and anthropogenic climate change. *J. Clim.* **24**, 3294–3308 (2011).
126. Osborne, M. C., Dunbar, R. B., Mucciarone, D. A., Druffel, E. & Sanchez-Cabeza, J.-A. A 215-yr coral δ^{18}O time series from Palau records dynamics of the West Pacific Warm Pool following the end of the Little Ice Age. *Coral Reefs* **33**, 719–731 (2014).
127. Ramos, R. D., Goodkin, N. F. & Fan, T.-Y. Coral records at the northern edge of the Western Pacific Warm Pool reveal multiple drivers of sea surface temperature, salinity, and rainfall variability since the end of the Little Ice Age. *Paleoceanogr. Paleoclimatol.* **35**, e2019PA003826 (2020).
128. Meehl, G. A. et al. in Climate Change 2007: The Physical Science Basis. Contribution of Working Group I to the Fourth Assessment Report of the Intergovernmental Panel on Climate Change Ch. 10 (eds Solomon S. et al.) 747–846 (Cambridge Univ. Press, 2007).
129. Tudhope, A. W. et al. Recent changes in climate in the far western equatorial Pacific and their relationship to the Southern Oscillation: oxygen isotope records from massive corals, Papua New Guinea. *Earth Planet. Sci. Lett.* **136**, 575–590 (1995).
130. McGregor, H. V. & Gagan, M. K. Western Pacific coral δ^{18}O records of anomalous Holocene variability in the El Niño–Southern Oscillation. *Geophys. Res. Lett.* **31**, L11204 (2004).
131. Asami, R., Quinn, T. M., Meyer, C. P. & Paulay, G. Interannual and decadal variability of the western Pacific sea surface condition for the years 1787–2000: Reconstruction based on stable isotope record from a Guam coral. *J. Geophys. Res.* **110**, C05018 (2005).
132. Quinn, T. M., Taylor, F. W. & Crowley, T. J. Coral-based climate variability in the Western Pacific Warm Pool since 1867. *J. Geophys. Res.* **111**, C11006 (2006).
133. Wu, H. C. & Grottoli, A. G. Stable oxygen isotope records of corals and a sclerosponge in the Western Pacific warm pool. *Coral Reefs* **29**, 413–418 (2010).
134. Hereid, K. A. et al. Coral record of reduced El Niño activity in the early 15th to middle 17th centuries. *Geology* **41**, 51–54 (2013).
135. Ramos, R. D., Goodkin, N. F., Siringan, F. P. & Hughen, K. A. *Diploastrea heliopora* Sr/Ca and δ^{18}O records from northeast Luzon, Philippines: An assessment of interspecies coral proxy calibrations and climate controls of sea surface temperature and salinity. *Paleoceanography* **32**, 424–438 (2017).
136. Ramos, R. D., Goodkin, N. F., Siringan, F. P. & Hughen, K. A. Coral records of temperature and salinity in the Tropical Western Pacific reveal influence of the Pacific Decadal Oscillation since the late nineteenth century. *Paleoceanogr. Paleoclimatol.* **34**, 1344–1358 (2019).
137. Linsley, B. K. et al. SPCZ zonal events and downstream influence on surface ocean conditions in the Indonesian Throughflow region. *Geophys. Res. Lett.* **44**, 293–303 (2017).
138. Murty, S. A. et al. Climatic influences on southern Makassar Strait salinity over the past century. *Geophys. Res. Lett.* **44**, 11967–11975 (2017).
139. Murty, S. A., Goodkin, N. F., Wiguna, A. A. & Gordon, A. L. Variability in coral-reconstructed sea surface salinity between the northern and southern Lombok Strait linked to East Asian Winter Monsoon mean state reversals. *Paleoceaongr. Paleoclimatol.* **33**, 1116–1133 (2018).
140. Cahyarini, S. Y. et al. Twentieth century sea surface temperature and salinity variations at Timor inferred from paired coral δ^{18}O and Sr/Ca measurements. *J. Geophys. Res.* **119**, 4593–4604 (2014).
141. Hennekam, R. et al. Cocos (Keeling) corals reveal 200 years of multidecadal modulation of southeast Indian Ocean hydrology by Indonesian throughflow. *Paleoceanogr. Paleoclimatol.* **33**, 48–60 (2018).
142. Meyers, G., McIntosh, P., Pigot, L. & Pook, M. The years of El Niño, La Niña, and interactions with the tropical Indian Ocean. *J. Clim.* **20**, 2872–2880 (2007).
143. Yang, Y. Seasonality and predictability of the Indian Ocean Dipole mode: ENSO forcing and internal variability. *J. Clim.* **28**, 8021–8036 (2015).
144. Zhang, W., Wang, Y., Jin, F.-F., Stuecker, M. F. & Turner, A. G. Impact of different El Niño types on the El Niño/IOD relationship. *Geophys. Res. Lett.* **42**, 8570–8576 (2015).
145. Stuecker, M. F. et al. Revisiting ENSO/Indian Ocean Dipole phase relationships. *Geophys. Res. Lett.* **44**, 2481–2492 (2017).
146. Nakamura, N. et al. Mode shift in the Indian Ocean climate under global warming stress. *Geophys. Res. Lett.* **36**, L23708 (2009).
147. Johnson, G. C. & Lyman, J. M. Warming trends increasingly dominate global ocean. *Nat. Clim. Change* **10**, 757–761 (2020).
148. Palmer, M. D. et al. Adequacy of the ocean observation system for quantifying regional heat and freshwater storage and change. *Front. Marine Sci.* **6**, 416 (2019).
Reviews the current status of ocean observing systems to quantify heat and freshwater changes across spatial and temporal scales.
149. Yu, L. et al. The global water cycle from atmospheric reanalysis, satellite, and ocean salinity. *J. Clim.* **30**, 3829–3852 (2017).
150. The Climate Change Initiative Coastal Sea Level Team Coastal sea level anomalies and associated trends from Jason satellite altimetry over 2002–2018. *Sci. Data* **7**, 357 (2020).
151. Rio, M.-H. & Hernandez, F. A mean dynamic topography computed over the world ocean from altimetry, *in situ* measurements, and a geoid model. *J. Geophys. Res.* **109**, C12032 (2004).
152. Maximenko, N. et al. Mean dynamic topography of the ocean derived from satellite and drifting buoy data using three different techniques. *J. Atmos. Ocean. Technol.* **26**, 1910–1919 (2009).
153. Rio, M. H., Guinehut, S. & Larnicol, G. New CNES-CLS09 global mean dynamic topography computed from the combination of GRACE data, altimetry, and in situ measurements. *J. Geophys. Res.* **116**, C07018 (2011).
154. Sen Gupta, A. et al. Climate drift in the CMIP5 models. *J. Clim.* **26**, 8597–8615 (2013).
155. Jourdain, N. C. et al. The Indo-Australian monsoon and its relationship to ENSO and IOD in reanalyses and the CMIP3/CMIP5 simulations. *Clim. Dyn.* **41**, 3073–3102 (2013).
156. Raghavan, S. V. et al. Assessment of CMIP5 historical simulations of rainfall over Southeast Asia. *Theor. Appl. Climatol.* **132**, 989–1002 (2018).
157. Toh, Y. Y. et al. Maritime Continent seasonal climate biases in AMIP experiments of the CMIP5 multimodel ensemble. *Clim. Dyn.* **50**, 777–800 (2018).
158. Pathak, R. et al. Precipitation biases in CMIP5 models over the south Asian region. *Sci. Rep.* **9**, 9589 (2019).
159. Pfeiffer, M. et al. 20th century δ^{18}O seawater and salinity variations reconstructed from paired δ^{18}O and Sr/Ca measurements of a La Reunion coral. *Paleoceanogr. Paleoclimatol.* **34**, 2183–2200 (2019).
160. Sanchez, S. C., Hakim, G. J. & Saenger, C. P. Climate model teleconnection patterns govern the Niño-3.4 response to early nineteenth-century volcanism in coral-based data assimilation reconstructions. *J. Clim.* **34**, 1863–1880 (2021).
161. Chan, D. et al. Correcting datasets leads to more homogeneous early-twentieth-century sea surface warming. *Nature* **571**, 393–397 (2019).
162. LeGrande, A. N. & Schmidt, G. A. Global gridded data set of the oxygen isotopic composition in seawater. *Geophys. Res. Lett.* **33**, L12604 (2006).
163. Breitkreuz, C. et al. A dynamical reconstruction of the global monthly mean oxygen isotopic composition of seawater. *J. Geophys. Res.* **123**, 7206–7219 (2018).
164. Durgadoo, J. V. et al. Indian Ocean sources of Agulhas leakage. *J. Geophys. Res.* **122**, 3481–3499 (2017).
165. van Sebille, E. et al. Pacific-to-Indian Ocean connectivity: Tasman leakage, Indonesian Throughflow, and the role of ENSO. *J. Geophys. Res.* **119**, 1365–1382 (2014).
166. Gordon, A. L. et al. Advection and diffusion of Indonesian throughflow water within the Indian Ocean South Equatorial Current. *Geophys. Res. Lett.* **24**, 2573–2576 (1997).
167. McPhaden, M. J. et al. RAMA: The research moored array for African–Asian–Australian monsoon analysis and prediction. *Bull. Am. Meteorol. Soc.* **90**, 459–480 (2009).
168. Kummerow, C. et al. The status of the Tropical Rainfall Measuring Mission (TRMM) after two years in orbit. *J. Appl. Meteorol.* **39**, 1965–1982 (2000).
169. Boutin, J. et al. New SMOS sea surface salinity with reduced systematic errors and improved variability. *Remote Sens. Environ.* **214**, 115–134 (2018).
170. Huang, B. et al. Improvements of the daily optimum interpolation sea surface temperature (DOISST) version 2.1. *J. Clim.* **34**, 2923–2939 (2020).
171. AVISO. *AVISO Level 4 Absolute Dynamic Topography for Climate Model Comparison. Version 1*. (PO.DAAC, 2011).
172. Yu, L., Jin, X. & Weller, R. A. Multidecade global flux datasets from the Objectively Analyzed Air-Sea Fluxes (OAFlux) Project: Latent and sensible heat fluxes, ocean evaporation, and related surface meteorological variables. Woods Hole Oceanographic Institution, OAFlux Project Technical Report (OA-2008-01), 64 pp (2008).
173. Dee, D. P. et al. The ERA-Interim reanalysis: Configuration and performance of the data assimilation system. *Q. J. R. Meteorol. Soc.* **137**, 553–597 (2011).
174. Zuo, H., Balmaseda, M. A., Tietsche, S., Mogensen, K. & Mayer, M. The ECMWF operational ensemble reanalysis–analysis system for ocean and sea ice: a description of the system and assessment. *Ocean Sci.* **15**, 779–808 (2019).
175. Adler, R. F. et al. The version-2 global precipitation climatology project (GPCP) monthly precipitation analysis (1979–present). *J. Hydrometeorol.* **4**, 1147–1167 (2003).
176. Rayner, N. A. et al. Global analyses of sea surface temperature, sea ice, and night marine air temperature since the late nineteenth century. *J. Geophys. Res.* **108**, 4407 (2003).
177. Huang, B. et al. Extended reconstructed sea surface temperature, version 5 (ERSSTv5): Upgrades, validations, and intercomparisons. *J. Clim.* **30**, 8179–8205 (2017).
178. Xie, P. & Arkin, P. A. Global precipitation: a 17-year monthly analysis based on gauge observations, satellite estimates, and numerical model outputs. *Bull. Am. Meteorol. Soc.* **78**, 2539–2558 (1997).
179. Fore, A. G., Yueh, S. H., Tang, W., Stiles, B. W. & Hayashi, A. K. Combined active/passive retrievals of ocean vector wind and sea surface salinity with SMAP. *IEEE Trans. Geosci. Remote Sens.* **54**, 7396–7404 (2016).
180. Ren, H. et al. 21st-century rise in anthropogenic nitrogen deposition on a remote coral reef. *Science* **356**, 749–752 (2017).
181. Rixen, T. et al. Impact of monsoon-driven surface ocean processes on a coral off Port Blair on the Andaman Islands and their link to North Atlantic climate variations. *Glob. Planet. Change* **75**, 1–13 (2011).

182. Abram, N. J. et al. Optimized coral reconstructions of the Indian Ocean Dipole: An assessment of location and length considerations. *Paleoceanography* **30**, 1391–1405 (2015).
183. Gagan, M. K. et al. Coral $^{13}C/^{12}C$ records of vertical seafloor displacement during megathrust earthquakes west of Sumatra. *Earth Planet. Sci. Lett.* **432**, 461–471 (2015).
184. Henley, B. J. et al. A tripole index for the interdecadal Pacific oscillation. *Clim. Dyn.* **45**, 3077–3090 (2015).
185. Buckley, B. M. et al. Interdecadal Pacific Oscillation reconstructed from trans-Pacific tree rings: 1350–2004 CE. *Clim. Dyn.* **53**, 3181–3196 (2019).
186. Reul, N. et al. Sea surface salinity estimates from spaceborne L-band radiometers: An overview of the first decade of observation (2010–2019). *Remote Sens. Environ.* **242**, 111769 (2020).
187. Adler, R. F. et al. The Global Precipitation Climatology Project (GPCP) monthly analysis (new version 2.3) and a review of 2017 global precipitation. *Atmosphere* **9**, 138 (2018).
188. Huffman, G. J. et al. The TRMM Multisatellite Precipitation Analysis (TMPA): Quasi-global, multiyear, combined-sensor precipitation estimates at fine scales. *J. Hydrometeorol.* **8**, 38–55 (2007).
189. Boutin, J. et al. Satellite and in situ salinity: understanding near-surface stratification and subfootprint variability. *Bull. Am. Meteorol. Soc.* **97**, 1391–1407 (2016).
190. Reynolds, R. W. et al. Daily high-resolution-blended analyses for sea surface temperature. *J. Clim.* **20**, 5473–5496 (2007).
191. Grottoli, A. G. & Eakin, C. M. A review of modern coral $\delta^{18}O$ and $\Delta^{14}C$ proxy records. *Earth-Sci. Rev.* **81**, 67–91 (2007).
192. Dunbar, R. B. & Wellington, G. M. Stable isotopes in a branching coral monitor seasonal temperature variation. *Nature* **293**, 453–455 (1981).
193. Urey, H. C. The thermodynamic properties of isotopic substances. *J. Chem. Soc.* https://doi.org/10.1039/JR9470000562 (1947).
194. Lough, J. M. & Cantin, N. E. Perspectives on massive coral growth rates in a changing ocean. *Biol. Bull.* **226**, 187–202 (2014).
195. Trenberth, K. E. & Olson, J. G. An evaluation and intercomparison of global analyses from the National Meteorological Center and the European Centre for Medium Range Weather Forecasts. *Bull. Am. Meteorol. Soc.* **69**, 1047–1057 (1988).
196. Parker, W. S. Reanalyses and observations: What's the difference? *Bull. Am. Meteorol. Soc.* **97**, 1565–1572 (2016).
197. Stammer, D., Balmaseda, M., Heimbach, P., Köhl, A. & Weaver, A. Ocean data assimilation in support of climate applications: Status and perspectives. *Annu. Rev. Mar. Sci.* **8**, 491–518 (2016).
198. IPCC. Annex I: Glossary. In Global Warming of 1.5 °C. An IPCC Special Report on the Impacts of Global Warming of 1.5 °C above pre-Industrial levels and Related Global Greenhouse Gas Emission Pathways, in the Context of Strengthening the Global Response to the Threat of Climate Change, Sustainable Development, and Efforts to Eradicate Poverty (eds Matthews, J. B. R.) (IPCC, 2018)
199. Li, Y. et al. Assessing the role of the ocean–atmosphere coupling frequency in the western Maritime Continent rainfall. *Clim. Dyn.* **54**, 4935–4952 (2020).

Acknowledgements
This work was supported by the US National Science Foundation under AGS-2002083 (to S.A.M. and C.C.U.), ICER-1663704 (to C.C.U.) and OCE-1851316 (to J.S.). C.C.U. also acknowledges support from the Andrew W. Mellon Foundation Award for Innovative Research and the James E. and Barbara V. Moltz Fellowship for Climate-Related Research, S.A.M. from the WHOI Postdoctoral Scholar Program and N.J.A. from the Australian Research Council through the Centre of Excellence for Climate Extremes (CE170100023) and a Future Fellowship (FT160100029). Part of this research was carried out at the Jet Propulsion Laboratory, California Institute of Technology, under a contract with the National Aeronautics and Space Administration. Graphic support from N. Renier (WHOI Graphics) is gratefully acknowledged.

Author contributions
C.C.U. and S.A.M. conducted the analyses and produced the figures. C.C.U., S.A.M., J.S., T.L. and N.J.A. wrote sections within the manuscript. All authors contributed to the discussion and commented on the manuscript.

Competing interests
The authors declare no competing interests.

Peer review information
Nature Reviews Earth & Environment thanks J. Vialard and the other, anonymous, reviewer(s) for their contribution to the peer review of this work.

Publisher's note
Springer Nature remains neutral with regard to jurisdictional claims in published maps and institutional affiliations.

Supplementary information
The online version contains supplementary material available at https://doi.org/10.1038/s43017-021-00192-6.